



Strål
säkerhets
myndigheten

Swedish Radiation Safety Authority

Technical Note

Review of recent research activities conducted by SKB relating to hydro-geological aspects of the disposal of radioactive waste

2024:13

Author: Joel Geier Clearwater Hardrock Consulting
Corvallis, Oregon, USA

Date: October 2024

Report number: 2024:13

ISSN: 2000-0456

Available at www.ssm.se



Strålsäkerhetsmyndigheten

Swedish Radiation Safety Authority

Author: Joel Geier Clearwater Hardrock Consulting
Corvallis, Oregon, USA

2024:13

Review of recent research activities conducted by SKB relating to hydrogeological aspects of the disposal of radioactive waste

Date: October 2024

Report number: 2024:13

ISSN: 2000-0456

Available at www.stralsakerhetsmyndigheten.se

SSM perspektiv

Bakgrund

Strålsäkerhetsmyndigheten (SSM) granskar Svensk Kärnbränslehantering AB:s (SKB) ansökningar i en stegvis prövnings- och godkännandeprocess enligt regeringens tillståndsvillkor enligt lagen (1984:3) om kärnteknisk verksamhet avseende uppförande, innehav och drift av geologiska slutförvarsanläggningar. Som en del i granskningen ger SSM konsulter uppdrag för att inhämta information i avgränsade frågor. I SSM:s Technical note-serie rapporteras resultaten från dessa konsultuppdrag.

Projektets syfte

Syftet med projektet var att granska och bedöma ett antal nyare forskningsaktiviteter som SKB genomfört och som är relevanta för hydrogeologiska aspekter av slutförvaring av radioaktivt avfall. Granskningen omfattar generell utveckling av SKB:s hydrogeologiska modelleringsförmåga samt detaljerade uppdateringar av modeller relevanta för planerade anläggningar i Forsmarksområdet.

Författarsammanfattning

Granskningen täcker följande huvudämnen:

- Framsteg med representationen av flera kopplade processer relaterade till grundvattenflöde under glaciala och periglaciala förhållanden. Det kan konstateras att en ambitiös utveckling har genomförts, men att modelleringsutmaningar kvarstår, till exempel i representationen av matrisdiffusion. Dessutom kan den övergripande betydelsen av glaciala och periglaciala scenarier för slutförvaringsystems säkerhet minska i ljuset av de senaste prognoserna av det framtida globala klimatet på 100 000 års tidsskalor.
- Utveckling av modelleringsmetoder för diskret spricknätverk (DFN). Specifika utvecklingar inom metodiken inkluderar: (1) demonstration av DFN-konditioneringsmetoder, av olika modelleringsgrupper med användning av två separata mjukvaruverktyg, (2) inkludering av bergspänningseffekter på sprickornas hydrauliska egenskaper, vilket pekar mot utveckling av en integrerad DFN-beskrivning av grund och djup berggrund i Forsmark, och (3) undersökning av inverkan av heterogena sprickor på transport i nätverksskala.
- Modellering av hydrologi i närfältet av slutförvaringsanläggningen för låg- och medelaktivt radioaktivt avfall, SFR. Det noteras att det har skett en relativt liten uppdatering av tidigare beräkningar, vilket återspeglar modifieringar av utformningen av den planerade utbyggnaden och antaganden om egenskaperna hos tekniska barriärer. Resultaten bedöms vara väl presenterade, på ett sätt som generellt tillåter direkt jämförelse med den tidigare modellen.

Projektinformation

Kontaktperson på SSM: Michael Egan
Diarienummer avrop: SSM2022-2334

Disclaimer: This report was commissioned by the Swedish Radiation Safety Authority (SSM). The conclusions and viewpoints presented in the report are those of the author(s) and do not necessarily coincide with those of SSM.

SSM perspective

Background

The Swedish Radiation Safety Authority (SSM) examines the Swedish Nuclear Fuel Company's (SKB) applications in a step-wise review and approval process according to the government's licence conditions under the Act on Nuclear Activities (SFS 1984:3) for the construction and operation of a geological disposal facilities. As part of the review, SSM commissions consultants to carry out work in order to obtain information on specific issues. The results from the consultants' tasks are reported in SSM's Technical Note series.

Objectives of the project

The objective of this project was to provide a review and assessment of recent research activities undertaken by SKB that are relevant to hydrogeological aspects of the disposal of radioactive waste. The scope incorporates general developments of SKB's hydrogeological modelling capabilities, as well as detailed updates of models relevant to planned facilities in the Forsmark area.

Summary by the author(s)

The review covers the following main topics:

- Advances in the treatment of multiple coupled processes relating to groundwater flow under glacial and periglacial conditions. It is noted that an ambitious development has been carried out, but that modelling challenges remain, for example as regards the representation of matrix diffusion. Furthermore, the overall significance of glacial and periglacial scenarios for disposal system safety may be declining against the background of the latest projections of future global climate on 100,000 year timescales.
- Development of the discrete-fracture network (DFN) modelling methods. Specific developments in the methodology include (1) demonstration of DFN conditioning methods, by modelling groups using two separate software tools, (2) incorporation of rock stress effects on the hydraulic properties of fractures, pointing towards development of an integrated DFN description of shallow and deep bedrock at Forsmark, and (3) examination of the influence of fracture inhomogeneity on network-scale transport.
- Modelling of near-field hydrology for the low- and intermediate-level radioactive waste disposal facility, SFR. It is noted that there has been a relatively minor update of previous calculations, reflecting modifications to the layout of the planned extension and assumptions regarding the properties of engineered barriers. The results are judged to be well-presented, in a way that generally allows for direct comparison with those of the previous model.

Project information

Contact person at SSM: Michael Egan

Contents

1. Introduction	2
2. Groundwater flow under glacial & periglacial conditions	3
2.1. Physical processes considered.....	5
2.2. Physical properties.....	7
2.2.1. Bedrock properties	7
2.2.2. Representation of subglacial layer	8
2.3. Boundary conditions and initial conditions	12
2.3.1. Boundary conditions.....	12
2.3.2. Initial conditions.....	14
2.4. Model predictions	15
2.4.1. Groundwater flux.....	15
2.4.2. Permafrost depths.....	17
2.4.3. Salinity and penetration of glacial meltwater	18
2.4.4. Role of taliks.....	19
2.5. Discussion.....	22
3. Development of DFN methodology	24
3.1. DFN-R Project.....	24
3.1.1. HypoSite model.....	24
3.1.2. Conditioning algorithms.....	25
3.1.3. Predicting flows to open deposition holes	27
3.1.4. Predicting post-closure performance measures.....	30
3.1.5. Discussion of results	32
3.2. Coupling of models to hydraulic stresses	33
3.2.1. Update of DFN model	33
3.2.2. Accounting for effects of rock stress on hydraulic aperture	37
3.2.3. Preliminary applications of new model	39
3.3. Effects of fracture heterogeneity on transport.....	40
3.3.1. Numerical experimental approach	41
3.3.2. Results	44
3.3.3. Comparison with previous SKB studies	45
3.4. Overall DFN Methodology.....	46
4. Near-field modelling for SR-PSU	49
4.1. Updates in model geometry and calculation cases.....	50
4.2. Results from updated model for SFR 1.....	51
4.3. Results from updated model for SFR 3.....	53
5. Summary of main findings	54
5.1. Modelling of glacial and periglacial conditions	54
5.2. Developments in DFN methods	54
5.2.1. Demonstration of DFN conditioning methods	55
5.2.2. Coupling of DFN models to hydraulic stresses	55
5.2.3. Effects of fracture heterogeneity on transport.....	56
5.3. Near-field modelling for SR-PSU	56
6. References	58

1. Introduction

This goal of this review is to give an up-to-date assessment of recent research activities by the Swedish Nuclear Fuel and Waste Management Company (SKB) that are relevant for hydrogeological aspects of disposal of radioactive waste. The scope of this review has been broad, taking into consideration general development of SKB's hydrogeological modelling capabilities, including treatment and understanding of situations that could arise in future climates, as well as detailed updates of models for planned facilities.

The review is structured in terms of the following main topics:

- Groundwater flow under glacial & periglacial conditions
- Development of discrete-fracture network (DFN) modelling methodology
- Modelling of the near-field hydrogeology for the low- and intermediate-level radioactive waste facility SFR.

These topics are dealt with in sequence in the following chapters.

2. Groundwater flow under glacial & periglacial conditions

Two of the reports considered in this review focused on modelling of groundwater flow below an ice sheet, based in part on data from the Kangerlussuaq region in Western Greenland, which has been the focus of the international Greenland Analogue Project (GAP), funded by SKB in cooperation with its counterparts, Posiva in Finland and NWMO in Canada.

General aims and results of the GAP were described by Harper et al. (2016) and Claesson Liljedahl et al. (2016), not reviewed here but considered as background information. The GAP considered the Greenland Ice Sheet as a present-day analogue for glaciation processes expected to reoccur in future glaciations in Fennoscandia and Canada.

The GAP study considered an approximately 12,000 km² area located east of Kangerlussuaq on the west coast of Greenland (Figure 2.1). Approximately 70% of the area (toward the east) is occupied by the ice sheet, while the remaining portion (toward the west) is not ice-covered, with permafrost in areas that are above sea level.

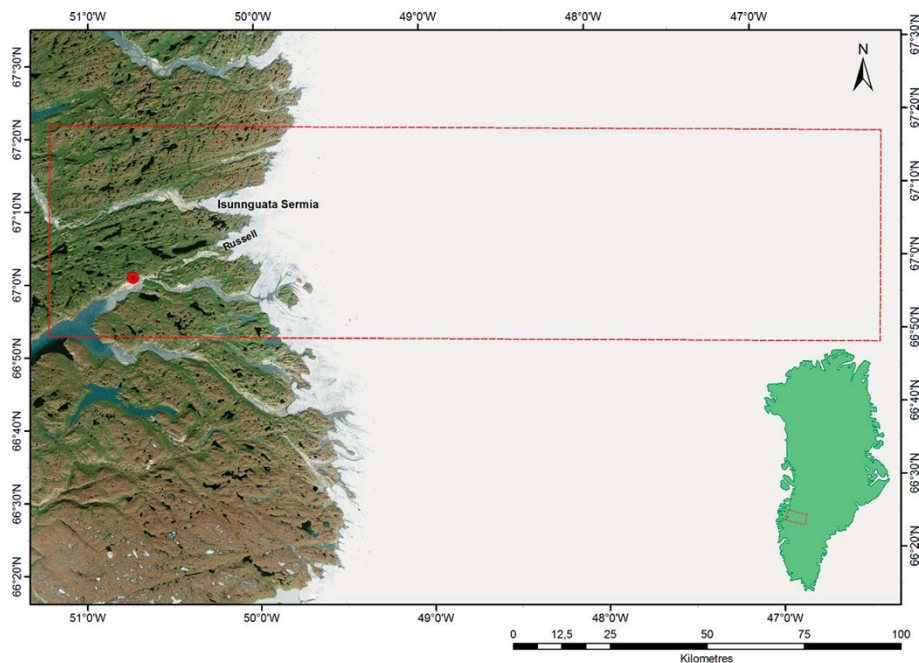


Figure 2.1: GAP study area (red dashed rectangle). Inset map shows the location of the study area on the Greenland scale. The key outlet glaciers in the GAP study area, Isunnguata Sermia and Russell glacier are indicated. Red circle shows the location of Kangerlussuaq village and the Kangerlussuaq International Airport (SFJ). Background image is a World Imagery Esri satellite image acquired 2 October 2014. From Figure 1-3 of Claesson Liljedahl et al. (2016).

GAP research activities as summarized by Claesson Liljedahl et al. (2016) included:

1. Surface-based ice sheet studies (mainly indirect observations from the ice sheet surface of the basal hydrological system),

2. Ice drilling and direct studies of basal conditions by drilling multiple drillholes at three locations up to 30 km from the terminus, to measure (a) thermal conditions within and at the base of the ice sheet; (b) generation of meltwater at the ice/bedrock interface; and c) hydrologic conditions at the base of the ice sheet.
3. Geosphere studies in deep and inclined boreholes through the permafrost in the vicinity of the ice, focusing on groundwater flow dynamics and the chemical and isotopic composition of water at depths of 500 metres or greater below ground surface, including evidence on the depth of permafrost, redox conditions and the infiltration of glacial meltwater into the bedrock.

Ground conditions under a proglacial lake were also investigated, to assess the potential role of *taliks* (areas of unfrozen ground within the permafrost) as pathways for exchange of deep groundwater and surface water.

The two reports reviewed here are:

- SKB R-15-01 Concept testing and site-scale groundwater flow modelling of the ice sheet marginal-area of the Kangerlussuaq region, Western Greenland (Vidstrand, 2017).
- SKB R-19-17 Groundwater flow modelling under transient ice sheet conditions in Greenland (Jaquet et al., 2019).

Both of these are modelling studies based on ice-sheet and topographic data from GAP, but using hydrogeologic properties based on sites that have been investigated as possible radioactive waste repository sites in Fennoscandia (Laxemar, Forsmark and Olkiluoto).

The work by Vidstrand (2017) can be seen as a preliminary version of the later model of Jaquet et al. (2019), using the same software and similar concepts, though with different modelling teams, so these are discussed together below.

These represent different scales and address different sub-objectives under the same overall modelling objective to: investigate the conditions and processes that impact the recharge of glacial melt water into the geosphere, in particular to repository depth in a fractured crystalline rock and over safety assessment time scales. For the model of Vidstrand (2017), the specific aims were to investigate the consequences of:

- different representations of a sub-glacial transmissive layer at the interface between the ice sheet and the geological substratum,
- the applied specified pressure at the top (bedrock) boundary of the modelled domain, and
- the extent of sub-glacial permafrost.

For the model of Jaquet et al. (2019), the focus was on more ambitious goals to improve the understanding of:

- regional groundwater flow system under ice sheet conditions during a complete glacial cycle;

- flow and infiltration conditions at the ice sheet bed;
- penetration depth of glacial meltwater into the bedrock;
- water chemical composition at repository depth in presence of glacial effects;
- role of the taliks, located in front of the ice sheet, likely to act as potential discharge zones of deep groundwater flow;
- influence of permafrost distribution on the groundwater flow system in relation to glacial periods of build-up, completeness and retreat;
- the applied specified pressure at the top (bedrock) boundary of the modelled domain; and
- the extent of sub-glacial permafrost.

The work by Jaquet et al. (2019) also builds on much earlier work by the same group (Jaquet et al. 2010 and Jaquet et al. 2012), not reviewed here.

Neither report gives a comparison with later data on flow at the ice/bedrock interface with data from the ICE project, as reported by Harper et al. (2021). Results are thus model projections (based on a reasonably well-controlled scenario for glacial advance and retreat), rather than tests of the predictive capabilities of these models.

2.1. Physical processes considered

The groundwater flow models reported by Vidstrand (2017) and Jaquet et al. (2019), are coupled thermal-hydraulic (T-H) analyses of the GAP study area. Both models are implemented in DarcyTools, which solves for coupled groundwater pressure and flow along with heat transport within the saturated bedrock and soil layers.

Advective-dispersive transport of salinity and coupled density-dependent flow effects were neglected in the model of Vidstrand (2017) which treated the entire system as freshwater, but included in the model of Jaquet et al. (2019).

Matrix diffusion, though supported by DarcyTools according to a multirate formulation given on p. 20-21 of Vidstrand (2017), was not used in that study and was omitted from the subsequent model of Jaquet et al. (2019) due to numerical problems. The problems with handling matrix diffusion appear to have been resolved, as a recent peer-reviewed article by Shahkarami and Sidborn (2023) describes and application of DarcyTools to model matrix diffusion of helium in a dual-continuum system.

Heat transport, both by conduction through the saturated, variably frozen medium and by fluid advection, is accounted for a coupled equation (Eq. 3-17 of Vidstrand, 2017) taking into account the latent heat of ice formation in the pore space. The DarcyTools implementation apparently allows for anisotropic thermal conductivity of the medium, but the method described for calculating the thermal conductivity of frozen ground (soil or bedrock) implies that isotropy was assumed.

Permafrost formation and thawing is accounted for by a mathematical relationship between temperature and ice fraction in the mobile pore space. The fraction of porosity with ice is related to temperature by an inverse exponential function of the form:

$$\epsilon = \epsilon_{max}[1 - \exp(-\beta\theta)]$$

where:

$$\beta_{\theta} = \left(\frac{\min(\theta, \theta_L) - \theta_L}{w} \right)^2$$

and where θ is temperature, θ_L is the thawing temperature, and w is an empirical thawing range for the material. Vidstrand (2017, p. 22) notes that “a thawing interval close to 0.1 provides good similarity between different laboratory data.” Effects of pressure changes on the freezing/thawing temperature of water in the pores are neglected.

The reduction in permeability due to freezing of pore water is accounted for by a power function:

$$k = \alpha k_{ref}$$

where:

$$\alpha = \max(\alpha_{min}, (1 - \epsilon)^{\alpha})$$

This is mathematically equivalent to the approach of Cohen-Corticchiato and Zwinger (2021), in a model of future glaciation at Olkiluoto, who account for the reduction in permeability with increasing ice fraction by scaling the reference permeability by a scalar factor α . Cohen-Corticchiato and Zwinger reported using α in the range 2 to 4 for soils, and $\alpha = 4$ for bedrock. Vidstrand (2017) does not report which value was used in the Kangerlussuaq model.

Formation or thawing of ice in the pores, combined with the difference in density between ice and liquid water, results in changes in the available pore volume for the remaining liquid water. Thus, changes in temperature results in displacement of water as the available pore space at a given point increases or decreases. This is accounted for as the second term in the following mass conservation equation (reformulated from Eq. 3-3 of Vidstrand, 2017):

$$\frac{\partial \rho_f \phi}{\partial t} + \frac{\partial (\rho_i - \rho_f) \epsilon \phi}{\partial t} + \nabla(\rho_f q) = Q$$

where ρ_f and ρ_i are fluid and ice densities, respectively, q is the Darcy flux, and Q is a source/sink term (Vidstrand expands the last term in terms of the directional components of the vector q but has an error in the expression for the z component).

Jaquet et al. (2019) use a slightly different formulation, which (adapting their equation 4-1 to the same notation) can be written as:

$$\frac{\partial \rho_f (1 - \epsilon) \phi}{\partial t} + \frac{\partial (\rho_i - \rho_f) \epsilon \phi}{\partial t} + \nabla(\rho_f q) = Q$$

where the first term appears to have been corrected for the reduction in porosity due to freezing of pore water.

2.2. Physical properties

The models of Vidstrand (2017) and Jaquet et al. (2019) consist mainly of two domains: the bedrock and a subglacial layer. Due to a paucity of site-specific data on bedrock properties for the west Greenland site even after conclusion of the GAP, properties are assigned based on data and interpretations from sites in Sweden (Laxemar and Forsmark) and Finland (Olkiluoto) that have been the subject of intensive investigations as potential sites for spent nuclear fuel repositories. Properties of the subglacial layer – treated as an interface between the bedrock and boundary conditions representing the overlying ice sheet – are largely speculative, based on measurements of subglacial pressures and their seasonal variation, observed in boreholes through the ice at a limited number of drilling sites as part of GAP.

2.2.1. Bedrock properties

Hydraulic and thermal properties of the bedrock are based on statistics for Laxemar, Forsmark, or Olkiluoto, depending on the model variant.

Vidstrand (2017) began with fracture statistics from Forsmark for the first stage of work, then switched to statistics from Laxemar as the geological setting of the GAP site was considered to be more similar to the Laxemar site than to Forsmark. Simulations of the fracture statistical model were upscaled to a discontinuous porous-medium equivalent model that preserves the main connective pathways formed by the fractures.

Jaquet et al. (2019) used a geostatistical description of Laxemar bedrock hydraulic conductivity for their main case and two parametric variants (which addressed a parameter controlling ice-sheet melting) but used Forsmark and Olkiluoto statistics for alternative cases. The geostatistical models for the respective cases are derived from upscaling of the respective discrete-fracture network models for each site to equivalent-continuum porous medium models.

On this bedrock model is superposed a set of deformation zones, interpreted based on geophysical lineament and geological mapping in the mostly exposed western part of the GAP area. Since the area covered by this interpreted set of deformation zones covers only part of the model domain, these deformation zones are duplicated for the remainder of the domain where the bedrock is entirely under the ice sheet so comparable data are unavailable (Figure 2.2).

Transmissivities of these deformation zones are assigned based on depth-dependent stochastic relationships as derived for the respective sites, given on p. 30 of Jaquet et al. (2019). A set of subhorizontal transmissive features in the shallow bedrock is also added to the model to mimic the presence of similar features seen at repository sites in Sweden and Finland.

For transport simulations, Jaquet et al. (2019) used kinematic porosity values calculated based on a logarithmic correlation to hydraulic conductivity given on p. 31, bounded to be within the range 0.0002 to 0.05.

Thermal conductivities of the bedrock are treated as homogeneous and isotropic throughout the domain, using average values for Laxemar, Forsmark or Olkiluoto

depending on the variant. Of these, Laxemar has the lowest thermal conductivity (2.75 W/m·K) and Forsmark the highest (3.45 W/m·K), while Olkiluoto is intermediate (2.91 W/m·K). Bedrock specific heat capacity is also treated as homogeneous, with values ranging from 1.93×10^6 J/m³·K (Olkiluoto) to 2.23×10^6 J/m³·K (Laxemar).

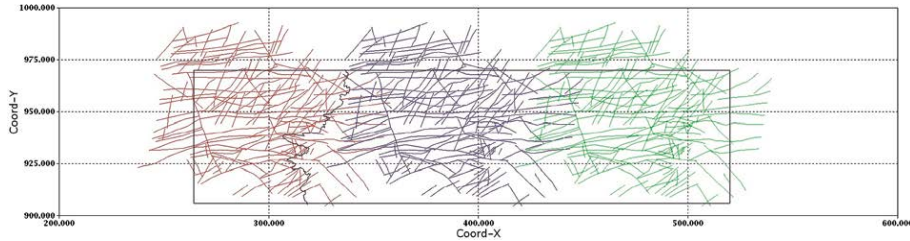


Figure 2.2: Replication of deformation zones from the mapped western portion of the GAP study area (shown as red lines) to the central and eastern portions (blue and green lines). The domain of the groundwater flow model is outlined as a black rectangle. The present-day ice margin is also indicated in black, near the east edge of the mapped portion (coordinates in kilometres). From Figure 5-6 of Jaquet et al. (2019).

2.2.2. Representation of subglacial layer

The effective upper boundary condition for these models is imposed at the ice-bedrock interface (for areas where the ice sheet is present at a given point in a glaciation cycle) or at the terrestrial-atmospheric interface (for the remaining portions). The treatment of the ice-bedrock interface in both models is largely speculative/exploratory, based on limited observations from the three widely separated sites where borehole investigations through the ice sheet were performed as part of the GAP.

In the Vidstrand (2017) model, the bedrock topography and ice thickness (which controls the imposed boundary conditions at the base of the ice) are based on downscaling data from digital elevation models (DEMs) for all of Greenland, with a 5 km resolution, for ice sheet basal topography and ice thicknesses. This approach, starting from such a coarse-resolution DEM, is unlikely to replicate actual topographic features such as valleys or ridges. But given the lack of higher-resolution data at the time of the study, it may be seen as a reasonable starting point for the limited purposes of a sensitivity study of the factors considered. Applicability for more site-specific analysis of subglacial hydrogeology is doubtful due to the limitation of the underlying DEMs for the modelling scale considered.

The subglacial layer is conceptualized as discontinuous permeable layer in a melted state at the bedrock/ice interface.

With an aim to produce a linked-cavity systems with different degrees of connectivity depending on the season, Vidstrand (2017) considered two alternative representations, produced by a fractal stochastic method and a Gaussian stochastic method (Figure 2.3). Both cases were hypothetical geometries rather than being constrained by high-resolution bedrock topographical data.

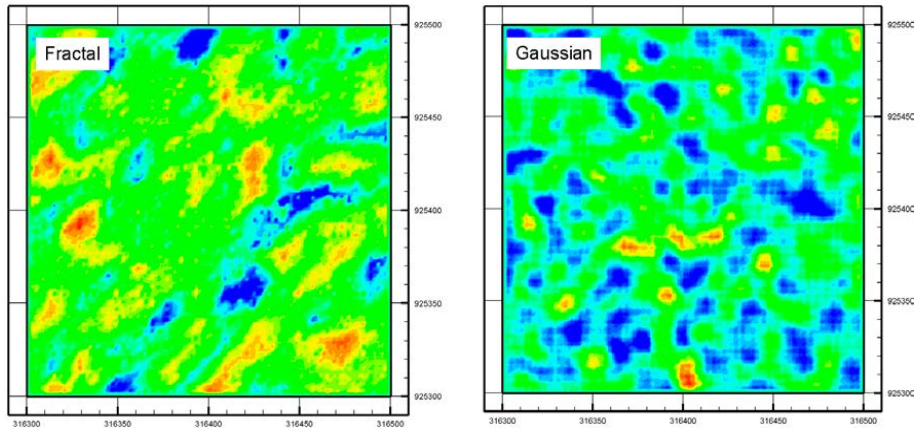


Figure 2.3: Alternative representations for subglacial layer considered by Vidstrand (2017) using fractal and Gaussian stochastic simulation methods to produce variably transmissive fields for a 200 m x 200 m area. Colours indicate the flow capacity of a subglacial transmissive layer, where red indicates a high and blue a low flow capacity. From Figure 4-09 of Vidstrand (2017).

Using the Gaussian representation, Vidstrand (2017) then applied numerical transformations to produce more- and less-connected conductivity fields within this 200 m x 200 m area (Figure 2.4). The more connected system is argued to be representative of summer conditions when higher recharge of meltwater occurs, while the less connective system could be more representative of winter months with less available meltwater. The resulting flow patterns when combined with the rest of the groundwater flow model are shown in Figure 2.5.

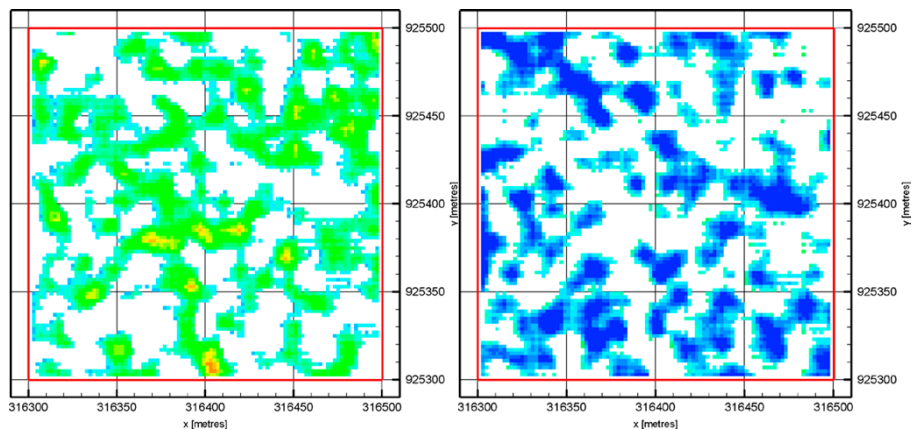


Figure 2.4: Transformed versions of the Gaussian stochastic field to produce (left) a more-connected basal flow system representative of summer conditions and (right) a less-connected basal flow system representative of winter conditions. Based on Figures 4-14 and 4-16 of Vidstrand (2017).

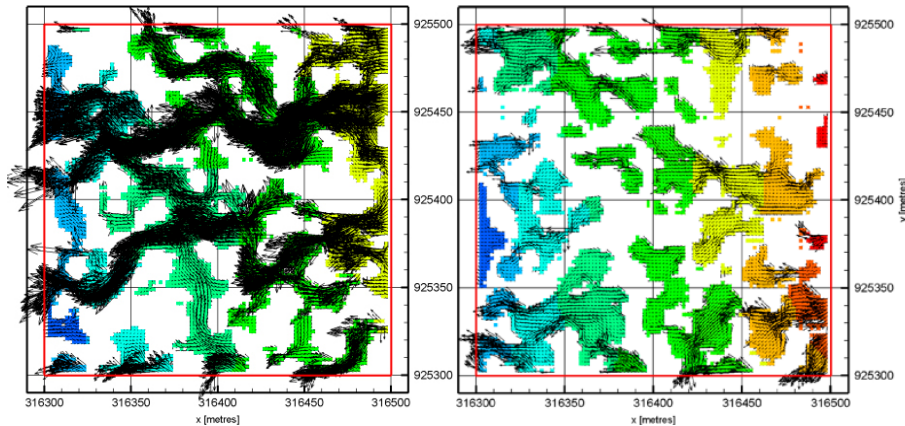


Figure 2.5: Simulated pressure and flow fields for water in the basal flow system in (left) a more-connected system representative of summer conditions and (right) a less-connected system representative of winter conditions. The colours indicate calculated groundwater pressures (red higher, blue lower) while the arrows indicate flow directions and magnitudes. Based on Figures 4-15 and 4-17 of Vidstrand (2017).

Vidstrand explored upscaling of this detailed representation of the subglacial layer to coarser grid scales, concluding that a coarser representation could be sufficient for models primarily focused on flow and related processes in the bedrock.

The model of Jaquet et al. (2019) takes a different approach to representing the subglacial layer, focusing on the large-scale representation. The available borehole data from the GAP, as discussed on p. 25 of their report, indicate that sediments below the ice sheet along transect extending 46 km east from the terminus are mostly thin (0 to 2 m) and are absent in some areas. However geophysical profiles and more localized borehole drilling has indicated a thick till layer elsewhere.

Based on interpretation of the limited data, Jaquet et al. (2019) adopt a model of the subglacial layer in which troughs and depressions in the bedrock topography are assumed to contain glacial till. High-resolution mapping of bedrock topography in the western part of the domain is extended by conditional geostatistical simulation to the eastern part.

The resulting bedrock topographic model (Figure 2.6) thus gives a true representation of the observed topography ahead of and near the edge of the ice sheet, but a synthetic topography to the east, which lacks some features of the observed topography (most noticeably, any tendency for continuity of topographic features in directions oblique to the main east-west trend).

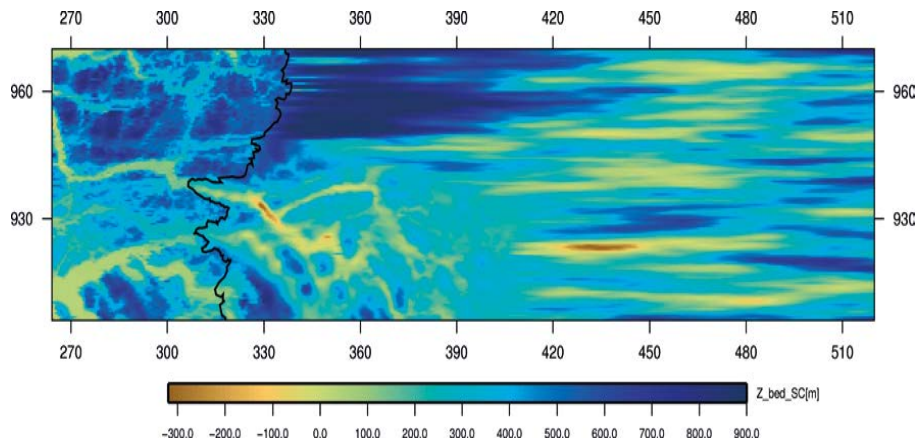


Figure 2.6: Bedrock elevation model based on high spatial resolution data in the western part of the domain (to the ice front near 332 km in the north, and farther inland to around 400 km in the south), extended farther inland to the east by conditional simulation for the remaining part of the domain. From Figure 5-9 of Jaquet et al. (2019).

The geometry of the subglacial layer was derived from the bedrock topographic model by treating all areas with bedrock surface elevation below 260 m elevation as part of the subglacial layer, with this layer being absent in areas of higher elevation. The choice of the 260 m threshold was chosen to preserve the main topographical troughs observed in the western part of the model.

An anisotropic hydraulic conductivity was assigned to this layer, with $K = 10^{-2}$ m/s in the horizontal directions and $K = 10^{-3}$ m/s in the vertical directions. For transport simulations, the kinematic porosity was assumed to be 0.25.

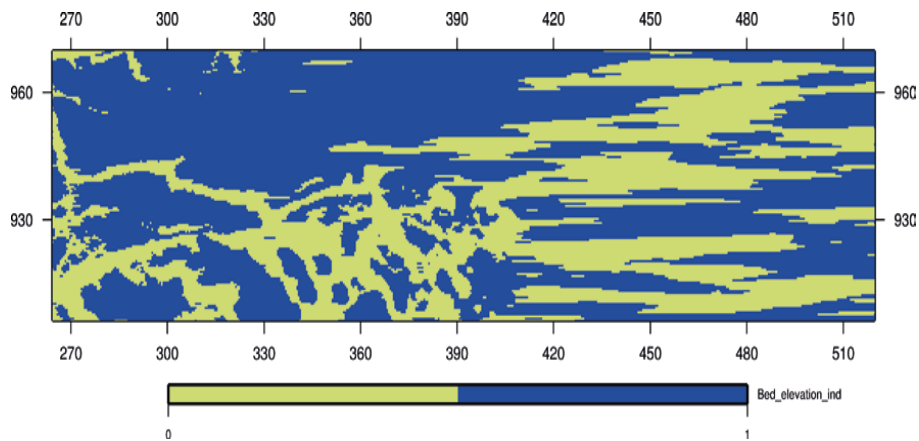


Figure 2.7: Geometry of the subglacial layer (yellow-grey colour) and areas where the subglacial layer is absent (blue). From Figure 5-10 of Jaquet et al. (2019).

2.3. Boundary conditions and initial conditions

2.3.1. Boundary conditions

Evaluating alternative boundary conditions for the top of the modelling domain was a main focus of Vidstrand (2017). Below the ice sheet, in the first phase of modelling (Part I) a specified recharge value (stated to be “high”) was imposed, except in regions of low bedrock hydraulic conductivity where a no-flow condition was imposed. Ahead of the ice sheet, a specified pressure was imposed.

In the second phase (Part II) a specified pressure was assigned, using pressures corresponding to a given percentage of the “overburden ice thickness (92, 70, 50, or 30%). This is not fully explained but presumably what is meant is that the pressure at the upper surface for a given point x is set to:

$$p_{BC}^{surface}(x) = f\rho_f g h_{ice}(x) + \rho_f g z$$

where $h_{ice}(x)$ is the local ice thickness and $f = 92, 70, 50,$ or 30% depending on the case. The highest of these values, 92% is approximately the ratio of ice density to water density. This a physical upper bound for the maximum pressure that could be sustained outside of dynamic situations where the ice is lifted upward by fluid pressure at the base.

Presence of permafrost is imposed as a thermal boundary condition as a specified ground-surface temperature below $0\text{ }^\circ\text{C}$, where the ice thickness is zero, or less than 100 m or 200 m in alternative parametric cases. Elsewhere below the ice, the temperature is set to $0.1\text{ }^\circ\text{C}$, representing pressure-melting conditions (noting again that effects of pressure on the freezing/melting point of water/ice are not treated explicitly in the model). The temperature below known taliks is set at $4\text{ }^\circ\text{C}$ so these remain open.

Jaquet et al (2019) used a specified pressure and considered time-dependent (rather than steady-state) ice thicknesses:

$$p_{BC}^{surface}(x,t) = \rho_{ice} g h_{ice}(x,t) + \rho_f g z$$

with ρ_{ice} being the density of ice, 917 kg/m^3 , which is roughly equivalent to the case of $f = 92\%$ considered by Vidstrand (2017).

The variation in ice thickness over time, for a given calculation case, is taken from a particular chosen simulation of the SICOPOLIS ice sheet model. Applegate et al. (2010) ran 100 SICOPOLIS simulations sampling the uncertainty ranges for five key parameters that are understood to control ice sheet build-up and retreat in that model:

- an *ice flow enhancement factor* which accounts for upscaling of ice rheological properties from the laboratory scale to ice-sheet scale;
- an *ice positive degree-day (PDD) factor* describing a statistical relation between surface temperatures and the rate of ice surface lowering (melting);

- a *snow PDD factor* describing an analogous statistical relation between surface temperatures and the rate of snow surface lowering (melting);
- the geothermal heat flux; and
- a *basal sliding factor* controlling rapidly the ice slides over its bed where the interface is not frozen.

Of these 100 simulations based on different parameter combinations, 27 were found to yield ice volumes within 10% of the modern ice volume in 2005 AD. All 27 of these simulations gave approximately steady ice thicknesses over the period -80 ka to -20 ka, so Jaquet et al. (2019) treated this period as steady-state in terms of ice sheet evolution. For calculation cases 1, 2, and 3 (representing base-case hydrogeological simulations for Laxemar, Forsmark, and Olkiluoto rock properties, respectively), one particular simulation from this ensemble was chosen which had an intermediate value of the PDD factor (Jaquet et al. do not clarify if this was the ice or snow PDD factor). For cases 4 and 5, different simulations from the ensemble were chosen which had lower and higher values of this factor, respectively.

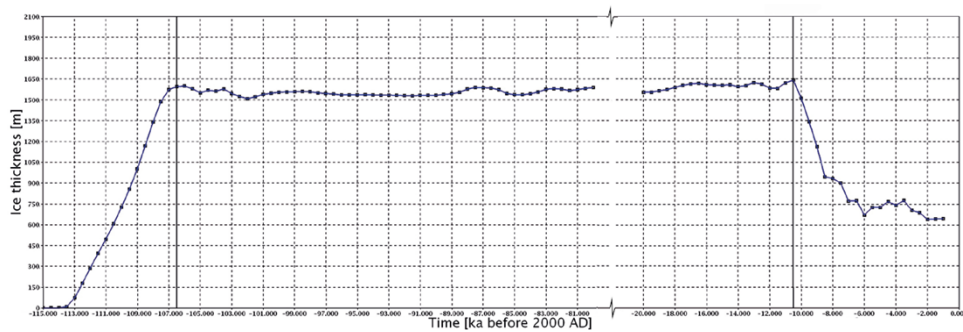


Figure 2.8: Evolution of mean ice sheet thickness over the model surface for -115 to -80 ka and -20 to -1 ka (note gap between periods), based on a SICOPOLIS simulation used for calculation cases 1, 2, and 3 of Jaquet et al. (2019). The vertical axis showing ice thickness ranges from 0 m to 2100 m. Based on Figures 6-11 and 6-12 of Jaquet et al. (2019).

Surface temperatures at the ground surface away from the ice sheet, for a given point in time, were also time-varying, specified based on long-term climate data derived from oxygen isotope ratios in ice core from the top of the Greenland ice sheet (Figure 2-9). Below the ice, the temperature is set to 0.1 °C, and the temperature below known taliks is set at 4 °C. These conditions are the same as imposed by Vidstrand (2017) except notably the entire area below the ice sheet is unfrozen, without the possibility for a frozen zone near the edge of the ice sheet where the ice thickness is less than 200 m.

For both models, the hydrogeological boundary conditions on the sides and at the base of the model (4 km deep) were no flow. Boundary conditions for salinity (modelled only by Jaquet et al.) are a prescribed concentration of 7.2% at the base of the model, fixed concentration $C = 0$ at the top of the model in areas covered by the ice sheet, and zero dispersive flux across the lateral boundaries or top boundary where the ice sheet is absent.

The thermal boundary conditions were zero heat flux on the lateral boundaries, and a specified geothermal heat flux of 0.0348 W/m² at the base of the model, based on GAP borehole data. Table 5-4 of Jaquet et al. (2019) lists a lower value of

geothermal heat flux (0.0234 W/m^2) for all three of the sites in Sweden and Finland, but it appears that the value obtained in west Greenland from GAP was used for all model variants.

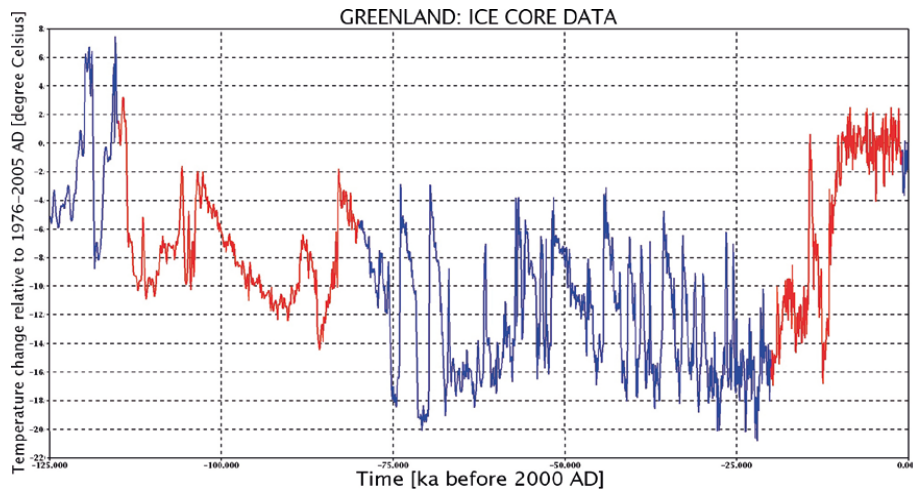


Figure 2.9: Temperature change based on ice-core data from central Greenland for times since -125 ka, relative to mean annual temperature for 1976–2005 AD. Data for the modelled periods (-115 to -80 ka and -20 to -1 ka) highlighted in red. Based on data from the joint European Greenland Ice-core Project (Dansgaard et al., 1993; Johnson et al., 1997), given as Figure 6-4 of Jaquet et al. (2019).

2.3.2. Initial conditions

Initial conditions for salinity used by Jaquet et al. (2019) depended on the modelling case considered, as detailed in Table 2.1. In all cases the initial temperature distribution in the model was set to $0 \text{ }^\circ\text{C}$ at ground surface and increasing with depth at a rate of $d\theta/dz = 0.015 \text{ }^\circ\text{C/m}$.

Table 2.1: Initial conditions for salinity and choice of glaciation scenario (based on value of positive degree-day factor) for the transient cases evaluated by Jaquet et al. (2019).

Case	Based on	Initial salinity C
1	Laxemar	$z \geq -150 \text{ m}$: $C = 0\%$ $-150 \text{ m} \geq z \geq -2100 \text{ m}$: increasing linearly $z \leq -2100 \text{ m}$: $C = 7.2\%$
2	Forsmark	$z \geq -350 \text{ m}$: $C = 0\%$ $-350 \text{ m} \geq z \geq -1500 \text{ m}$: increasing linearly $z \leq -1500 \text{ m}$: $C = 7.2\%$
3	Olkiluoto	$z \geq -30 \text{ m}$: $C = 0\%$ $-30 \text{ m} \geq z \geq -400 \text{ m}$: increasing linearly $z \leq -400 \text{ m}$: $C = 8.1\%$
4	Laxemar	same as Case 1
5	Laxemar	same as Case 1

2.4. Model predictions

The investigations of Vidstrand (2017) were aimed mainly at testing concepts and methods that might be applied in further modelling. Key findings include:

- Support for use of specified-pressure top boundaries as providing reasonable results relative to more complicated upper boundary conditions.
- Identification of a need for more detailed representation of local topography and potential for sub-glacial permafrost.
- Identification of a need for detailed resolution if details of sub-glacial groundwater flow and melt water transport are an aim of investigation.
- Indications of the importance of taliks in the periglacial environment potentially both as discharge zones glacial melt water and for recharge to the deeper groundwater system, including a possibility for different parts of taliks to function simultaneously as recharge and discharge areas.

Performance measures calculated by Jaquet et al. (2019) include:

- groundwater flux,
- depth of permafrost,
- salinity, and
- concentrations of glacial meltwater at taliks.

The main results are summarized and discussed briefly below.

2.4.1. Groundwater flux

Jaquet et al. (2019) present the calculated groundwater fluxes visually as maps of Darcy velocities in both the top layer of the model (subglacial layer) and at $z = -500$ m.a.s.l. (a representative depth for a spent-fuel repository), as well in terms of average recharge/discharge fluxes through various horizons in the domain. These are presented for three main stages of glaciation: glacial absence (-114 ka), glacial completeness (-102 ka), and glacial retreat (-9 ka). The last of these stages is discussed here as the most interesting for repository safety assessment, as a period when relatively high fluxes can be expected near the edge of the ice sheet.

Darcy velocities in the top layer of the model, as shown for Case 1 in Figure 2.10, indicate concentration of flow in the topographic lows where the subglacial layer is present and minimal flow elsewhere in the uppermost bedrock.

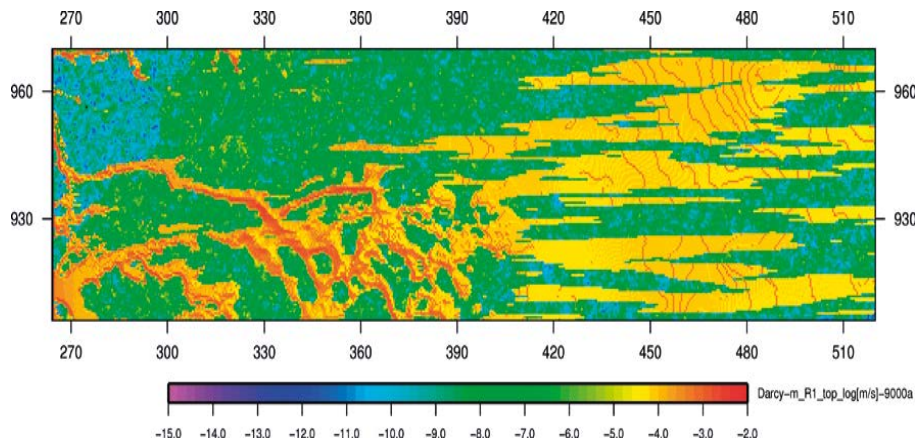


Figure 2.10: Darcy velocities (log [m/s]) in the top layer of the model at -9 ka during the period of glacial retreat for Case 1 (Laxemar bedrock properties). From Figure 6-38 of Jaquet et al. (2019).

The reddish lines running transverse to the main east-west orientation of these flowing zones in the eastern part of the domain in Figure 2.10, giving the appearance of contour lines, are not discussed in the text. Similar lines appear in the identical positions for the corresponding plots of other stages of glaciation, so apparently they are not related to ice sheet thickness or the corresponding pressure boundary condition applied at the top of the model. These might be numerical artifacts resulting from steps in the representation of the bedrock topography.

The Darcy velocities at $z = -500$ m.a.s.l. for the same case (Figure 2.11) vary over about 4 orders of magnitude, reflecting the heterogeneity of the bedrock representation. Relatively high values are apparent from a preponderance of red and yellow tones in the western part of the model, near the edge of the ice sheet.

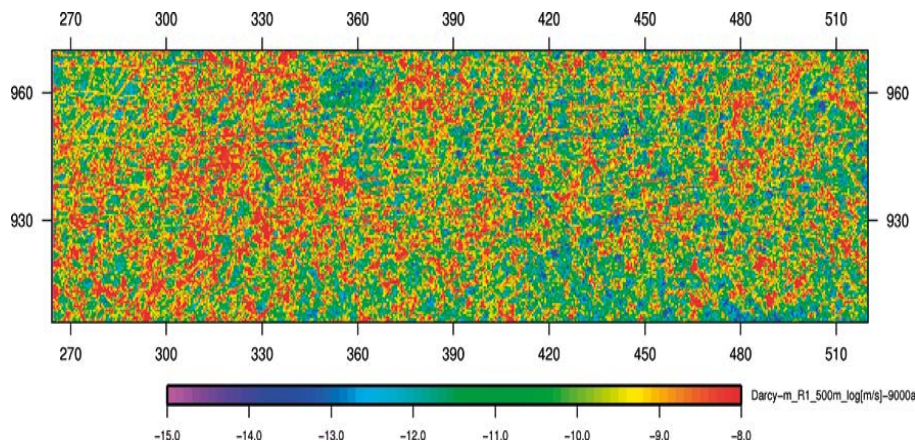


Figure 2.11: Darcy velocities (log [m/s]) at -500 m.a.s.l. at -9 ka during the period of glacial retreat for Case 1 (Laxemar bedrock properties). From Figure 6-41 of Jaquet et al. (2019).

Average values of groundwater recharge and discharge flux for a given stage of glacial build-up or retreat are calculated as averages over the entire domain (for a given elevation), for slices through the model on a 100 m spacing from $z = -200$ m down to -1000 m. The results, as presented in Section 7.1 of Jaquet et al. (2019), are not especially informative for assessing fluxes for a specific repository location at a

given distance from the edge of an ice sheet. For future site-specific applications in safety assessment, this type of performance measure would presumably be calculated for a smaller portion of the model corresponding to the repository location, rather than averaged over the entire domain.

2.4.2. Permafrost depths

Permafrost depths are presented both as cross-section plots at selected points in time and in terms of statistics (mean, standard deviation, and percentiles) over the domain for stages of glacial build-up and retreat.

The model predicts deeper permafrost penetration at Forsmark compared to Laxemar during glacial build-up but shallower penetration at Forsmark during glacial retreat (Figures 2.12 and 2.13). Jaquet et al. (2019) attribute this to the relatively high contrast of hydraulic conductivity values in the shallow vs. deep bedrock at Forsmark, which they argue limits the ability of water to transfer colder temperatures to depth.

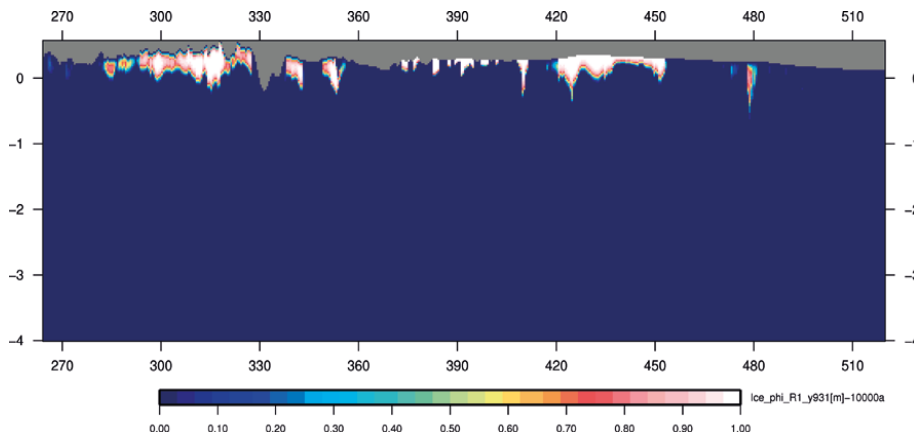


Figure 2.12: Vertical E-W cross-section at -10 ka (permafrost expressed as ice proportion) for Case 1 (Laxemar bedrock properties). From Figure 6-46 of Jaquet et al. (2019).

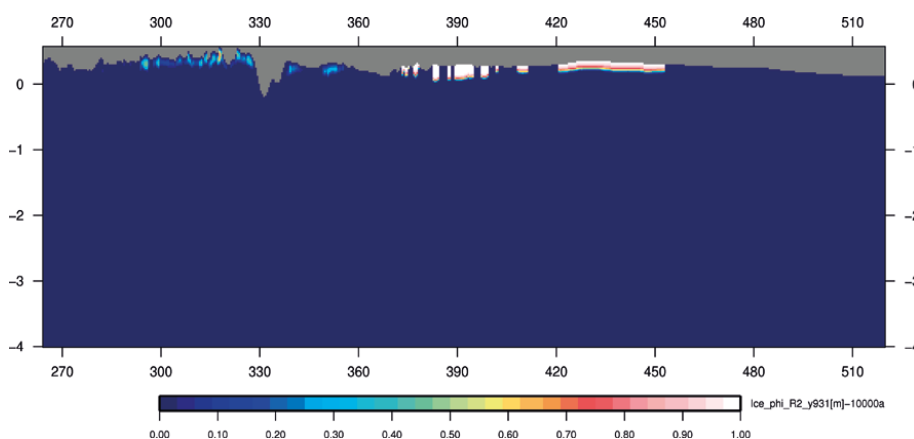


Figure 2.13: Vertical E-W cross-section at -10 ka (permafrost expressed as ice proportion) for Case 2 (Forsmark bedrock properties). From Figure 6-45 of Jaquet et al. (2019).

The limited role of advective heat transport at Forsmark is supported by analysis of the parameters governing transport of heat at Forsmark. As suggested in a review of

a draft of this report (personal communication, Roy Haggerty, March 2023), this can be considered in terms of the Nusselt number which describes the ratio of total heat transfer (including advection) to the heat transfer that would be expected in the absence of advection:

$$Nu = \frac{\text{advective heat transport} + \text{conductive heat transport}}{\text{conductive heat transport}}$$

which can be written (Ingebritsen et al., 2006)

$$Nu = \frac{c_w \rho_w q_w T + K_m \frac{\Delta T}{L}}{K_m \frac{\Delta T}{L}}$$

where c_w is the specific heat capacity of water, ρ_w is water density, q_w is the advective flux, T is the absolute temperature, K_m is the bulk thermal conductivity of the rock mass, and $\Delta T/L$ is the vertical temperature gradient. A value close to unity indicates negligible influence of advective heat transport, while higher values indicate that advective heat transport via flowing groundwater could be significant.

Assuming that the length scale for advection is the same as the length scale L for heat conduction and substituting in Darcy's law for q_w , this can be simplified to:

$$Nu = \frac{c_w \rho_w K \Delta h + K_m \Delta T / T}{K_m \Delta T / T}$$

Assuming a hydraulic head gradient of 0.004 acting over a vertical length scale of 200 m to give $\Delta h = 0.8$ m, and a temperature gradient of 3 °C over the uppermost 200 m, with typical values of thermal conductivity (3.45 Wm⁻¹K⁻¹ for Forsmark and 2.75 Wm⁻¹K⁻¹ for Laxemar) and hydraulic conductivity (3x10⁻¹¹ m/s for the deep bedrock and Forsmark, 2x10⁻⁹ m/s for the shallow bedrock at Forsmark, and 1x10⁻⁷ m/s for the shallow bedrock at Laxemar) leads to the following Nusselt numbers:

Forsmark (deep): $Nu = 1 + 0.0028$ (advection negligible)

Forsmark (shallow): $Nu = 1 + 0.2$ (advection may play minor role)

Laxemar (shallow): $Nu = 1 + 12$ (advection dominant)

This simple analysis appears to confirm that the results of this model are reasonable, in terms of the differences in permafrost penetration between Forsmark and Laxemar. The results may also be sensitive to the geothermal gradient applied at the base of the model, which is based on data from west Greenland rather than Fennoscandia.

2.4.3. Salinity and penetration of glacial meltwater

The model of Jaquet et al. (2019) predicts very deep penetration of dilute glacial meltwater down to depths of 2 km or more during glacial retreat, both for the case based on Laxemar bedrock properties (Figure 2.14) and for the case based on Forsmark bedrock properties (Figure 2.15). The realism of these results is doubtful, for two reasons:

- Bedrock hydrogeologic properties (except for within fracture zones) are statistically homogeneous with depth.
- Matrix diffusion has not been included in the model.

The first issue is an artifact of how hydrogeological interpretations from the sites in Sweden and Finland have been transferred to this particular model. The hydrogeological site descriptive models for Laxemar, Forsmark, and Olkiluoto all imply strongly decreasing hydraulic conductivity at depths of more than a few hundred metres, which inhibits flow circulation to the types of depths implied by this model. Diffusive exchange between infiltrating glacial meltwater and more saline waters in the rock matrix would be expected to further attenuate the propagation of dilute conditions to repository depth. Scoping calculations are suggested to bound these effects.

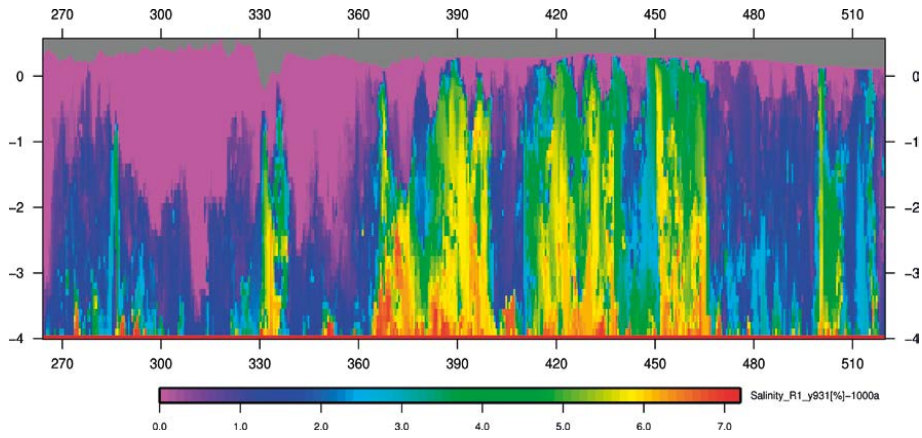


Figure 2.14: Salinity during glacial retreat for case 1 (Laxemar bedrock properties). From Figure 6-34 of Jaquet et al. (2019).

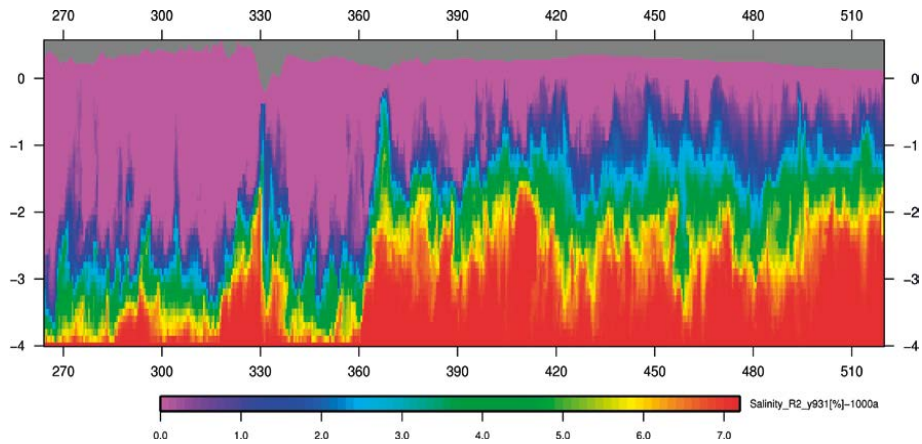


Figure 2.15: Salinity during glacial retreat for case 2 (Forsmark bedrock properties). From Figure 6-50 of Jaquet et al. (2019).

2.4.4. Role of taliks

Permafrost in the periglacial environment ahead of an advancing ice sheet mainly acts as a barrier to groundwater flow, so discharge of flows through repository depths would be inhibited by thicker permafrost. However taliks (areas of unfrozen ground in permafrost) may provide paths for focused discharge.

Jaquet et al. (2019) include taliks in the model, based on locations of present-day taliks. The taliks are kept open by a prescribed temperature of 4 °C when not under the ice sheet. Their results indicate that only taliks within a few kilometres of the ice

front will discharge glacial meltwater (Figures 2.16 and 2.17). Taliks farther ahead of the ice front are indicated to have a minimal glacial meltwater component.

More recent work by Cohen-Corticchiato and Zwinger (2021) includes a mechanism for taliks to form dynamically. The model is very computationally demanding, which has limited its application thus far to just a small set of site-scale simulations for Olkiluoto. In those simulations, taliks are predicted to form where the ground surface is characterized by peat, surface water, and/or high values of a terrestrial water index. These factors are likely correlated to topography in the present-day landscape, so use of fixed locations by Jaquet et al (2019) may be reasonable.

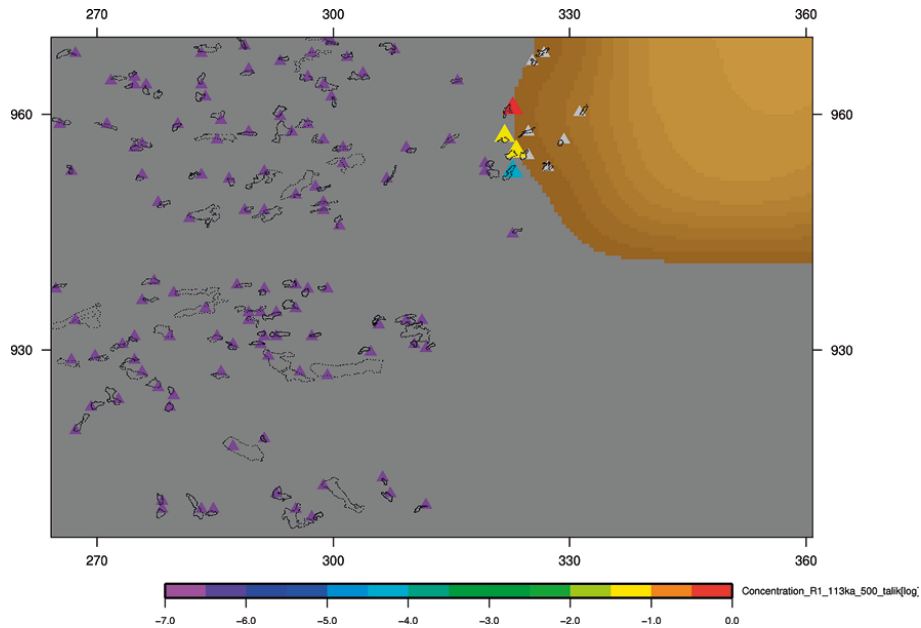


Figure 2.16: Discharge of glacial meltwater (expressed as a concentration relative to total groundwater discharge) to taliks ahead of the ice sheet during glacial build-up (~113 ka). From Figure 7-27 of Jaquet et al. (2019).

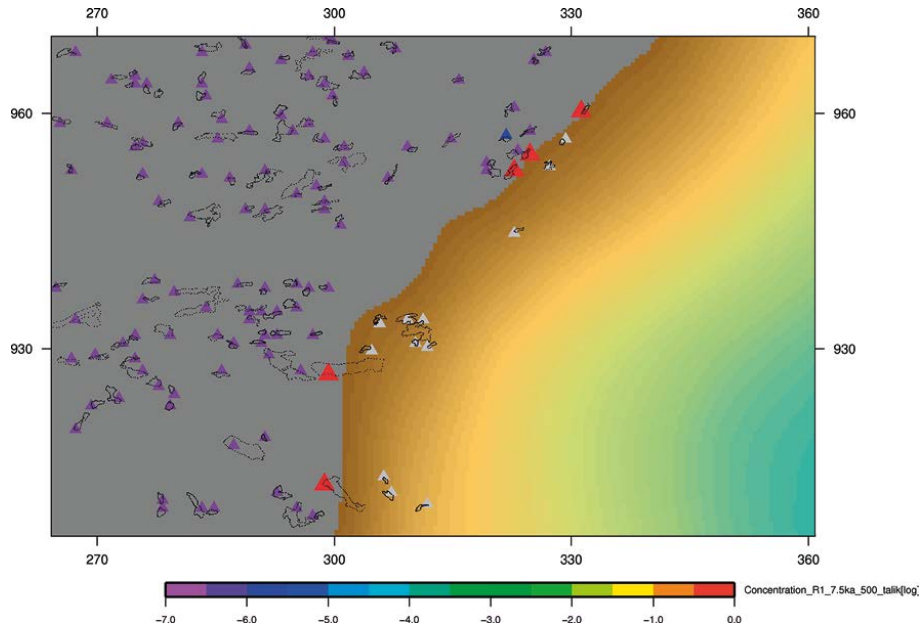


Figure 2.17: Discharge of glacial meltwater (expressed as a concentration relative to total groundwater discharge) to taliks ahead of the ice sheet during glacial retreat (-9 ka). From Figure 7-28 of Jaquet et al. (2019).

2.5. Discussion

The model of Jaquet et al. (2019), in particular reflects an ambitious level of model development using the DarcyTools software to incorporate most of the major physical processes that are expected to be relevant for groundwater flow in glacial and periglacial situations. The most notable omission is matrix diffusion, which was omitted from the calculations reportedly due to numerical difficulties. Unfortunately these numerical problems are not discussed in any detail by the authors, leaving an open question as to the source of the problems and whether these problems could be resolved in future analyses of glacial and periglacial situations.

The application to the west Greenland analogue site is hindered by limited site-specific characterization, especially of the bedrock at repository depths and for areas still covered by the ice sheet. The application is thus necessarily schematic compared with what would be expected for site-specific safety assessments.

The overall significance of glacial scenarios for a repository safety case may be waning in view of current projections of future climates. Recent climate evolution modelling by Lord et al. (2019) and Williams et al. (2022), indicates that the timing of the next glacial inception will be strongly affected by anthropogenic CO₂ emissions, possibly to a greater degree than has been recognized in past safety assessments for radioactive waste repositories (Figure 2.18).

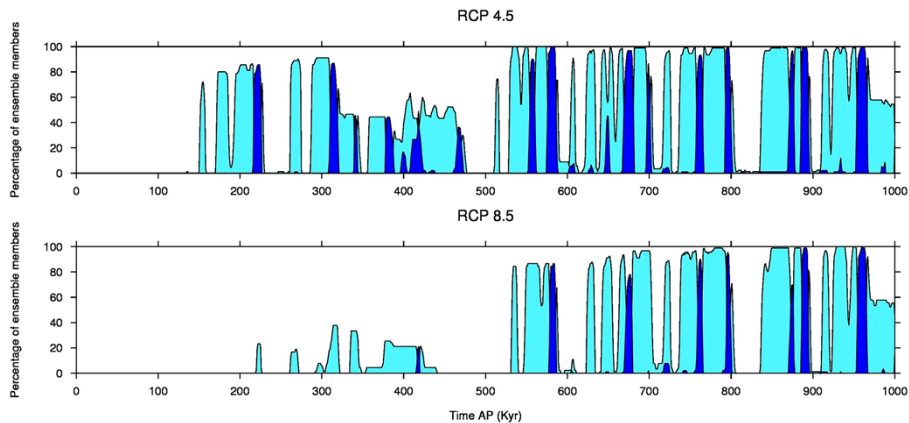


Figure 2.18: Probability of climate going into cold (-8 to -15 °C, light blue) and very cold (below -15 °C, dark blue) regimes at Forsmark for RCP 4.5 and RCP 8.5 carbon emission scenarios (Williams et al., 2022).

According to Lord et al. (2019), a low to medium emissions scenario (IPCC 2014 carbon emissions scenario RCP 4.5 plus relatively fast declines in atmospheric CO₂) – which might now be regarded as optimistic given limited progress in curbing carbon emissions worldwide – implies that:

- The next glacial inception occurs in about 50,000 years, and
- The first ice sheet coverage at Forsmark or Olkiluoto occurs around 100,000 to 130,000 years after the present.

Relatively high emissions (IPCC 2014 carbon emissions scenario RCP 8.5 plus relatively slow declines in atmospheric CO₂) – which might now be regarded as realistic – imply (Lord et al., 2019):

- The next glacial inception occurs in about 170,000 years, and
- The first ice sheet coverage at Forsmark or Olkiluoto does not occur until around 410,000 year after the present.

Thus, periglacial and glacial periods are unlikely to occur within the early part of the period considered for safety assessments in the Swedish regulatory context, unless there is a much more rapid reduction in anthropogenic CO₂ emissions combined with implementation of new technologies for CO₂ removal and sequestration.

The possibility of an extended temperate period due to anthropogenic carbon emissions has been recognized as a scenario in previous safety assessments by SKB, including the SR-Site safety assessment for Forsmark. The significance of the recent work by Lord et al. (2019) and Williams et al. (2022) is the conclusion that this scenario appears to be more likely, based on the continuing trajectory of global carbon emissions.

3. Development of DFN methodology

Five reports published by SKB in recent years and considered here are related to developments in discrete-fracture network (DFN) modelling methodology. These are discussed in terms of the following four categories in separate sections of this chapter:

- Developing and testing methods of conditioning DFN models to observations in tunnels and boreholes.
- Extensions to hydrogeological DFN models to account for rock stress and reactive transport.
- Evaluation of the effects of channelling in DFN models.
- General compilation of DFN methodology

The five reports are discussed in terms of above categories in the following subsections.

3.1. DFN-R Project

SKB's DFN-R project is aimed at developing a DFN methodology to produce conditional simulations of DFN statistical models that honour measured data (both geological and hydrogeological) from tunnels and boreholes, for models on the repository scale.

Two reports within the DFN-R project are considered here:

- SKB R-17-11. Conditioning DFN models on intersection, connectivity and flow data (Appleyard et al., 2017).
- SKB R-17-12. Methods and workflow for geometric and hydraulic conditioning. DFN-R – status report 2013–2015 (Bym and Hermanson, 2017).

Both of these studies used synthetic data from a numerical realisation of a hypothetical site, referred to as HypoSite.

3.1.1. HypoSite model

HypoSite is a fracture network model for an 800 m × 800 m × 800 m cubical volume around a section of a hypothetical repository which includes a horizontal main tunnel and two horizontal deposition tunnels that cross the main tunnel, with room for 32 deposition holes sized and spaced in accordance with SKB's design criteria for a spent-fuel repository based on the KBS-3V concept (Figure 3.1).

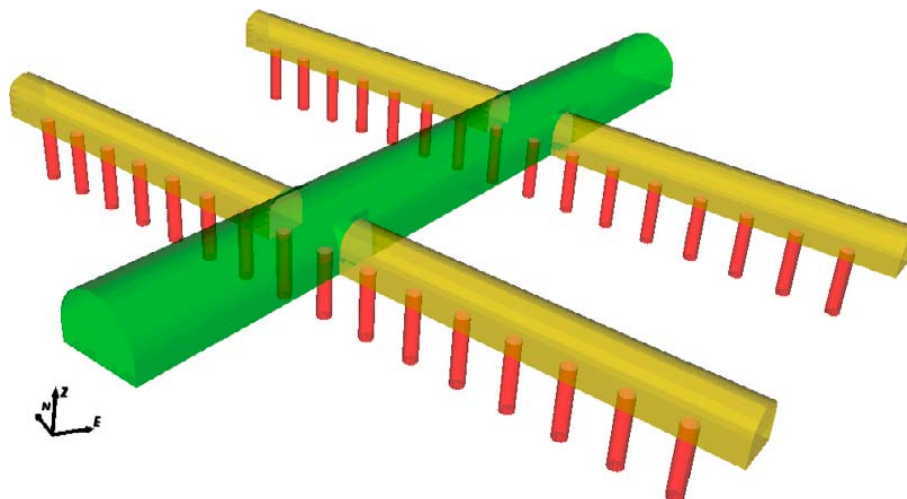


Figure 3.1: Image of the hypothetical tunnels and deposition holes in HypoSite. The main tunnel is in green, the deposition tunnels are in yellow and the deposition holes are in red. From Figure 3-1 of Appleyard et al. (2017).

Fractures in the HypoSite model are synthetically generated from a relatively simple DFN statistical description with just three fracture sets, each described by a Fisher distribution. Fractures are assumed to have uniform transmissivity across their areas (i.e. no channelling). The significance of this idealisation was not explored within the DFN-R project. However the subsequent results of Bym and Follin (2019), as discussed in Section 3.3 of this review, suggest that it may be significant for some applications of DFN models in a repository context.

The model is divided into two domains across a vertical plane bisecting the main tunnel. These domains have slightly different fracture intensities (differing by about 30% at a given depth). The overall fracture intensity of $1.95 \text{ m}^2/\text{m}^3$ is nominally comparable to the total fracture intensity of the bedrock at Forsmark. Within each domain, fracture intensity decreases monotonically with depth, so fracture intensity decreases from about 3 to $4 \text{ m}^2/\text{m}^3$ at the top of the model to less than $1 \text{ m}^2/\text{m}^3$ at repository depth.

Ten realizations of fractures based on this DFN statistical model, numbered 1 through 10 were produced and provided to the modelling teams to use as synthetic versions of the "true" fractures in the HypoSite model volume. Of these, realization number 4 was adopted as the preferred realization because it has the largest number of deposition holes that are connected to the external surfaces of the model.

3.1.2. Conditioning algorithms

The goal of both studies was to use data that could be obtained locally from tunnels and deposition holes within the HypoSite model – for example, fracture traces on the simulated tunnels and simulated hydraulic measurements in pilot holes – to produce conditional realizations of the DFN model that could then be used to make local hydrogeological predictions, and to assess the accuracy of those predictions versus the synthetic "true" system.

Appleyard et al. (2017) used Connect Flow (proprietary software of Amec Foster Wheeler, now owned by Wood Group) in their approach to this problem. Bym and Hermanson (2017) used FracMan (proprietary to Golder Associates, now owned by WSP Global Inc.).

There are minor differences in the implementation due to differences in the geometrical representation of fractures in ConnectFlow (as rectangles or right triangles) versus FracMan (as arbitrary n -sided polygons, commonly hexagons or dodecagons).

The algorithms for conditional simulation of fracture geometries also differ between the two models. In ConnectFlow, a simulation of a very large number of fractures is used to calculate intersections with a given set of underground openings (such as tunnels, rooms, boreholes or deposition holes), keeping track of the intersection geometries in a "library" of fractures. A conditional simulation is then produced by selecting the fractures from that library that most nearly match the intersections observed in reality, together with randomly generated fractures that do not intersect any of the underground openings. Criteria taken into account in selecting fractures from this "library" include both geometrical properties (such as orientation) and connectivity/flow categories.

In the FracMan application described by Bym and Hermanson (2017), a "fracture replacement" method is used, in which fractures from an unconditional realization of the DFN are shifted into positions that reproduce the observed intersections with underground openings. This algorithm is explained in detail in Chapter 2 of the report. Both this and the "library" method used in ConnectFlow are capable of conditioning DFN realizations in cases where fractures may be mapped in more than one underground opening.

The matches between simulated and "observed" (synthetic) fracture traces with the "library" algorithm used in ConnectFlow are not exact but are reasonably close (Figure 3.2). With the "fracture replacement" algorithm used in FracMan, the match is effectively exact, at least for the idealized case considered in this exercise, where the "observed" fractures are planar (Figure 3-3).

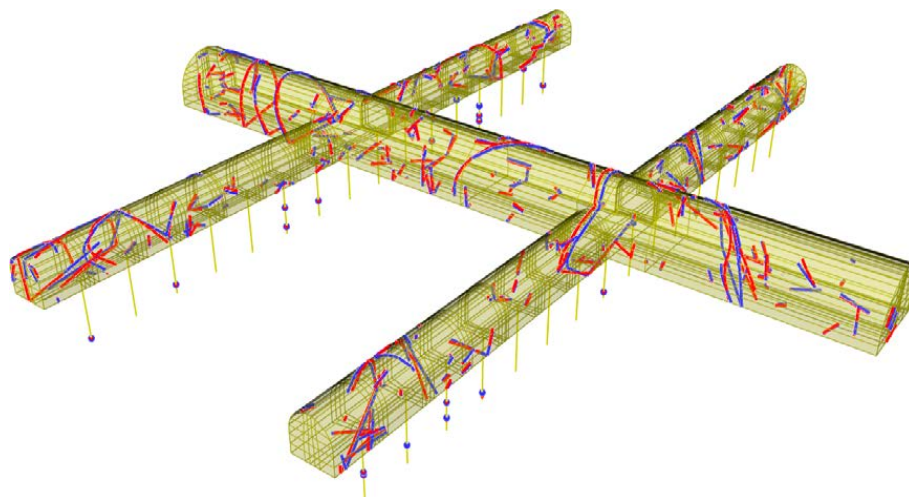


Figure 3.2: Comparison between fractures observed (blue) and added through conditioning (red) for a model conditioned without flow for Realization 4 of HypoSite case BM-1b. From Figure 3-6 of Appleyard et al. (2017).

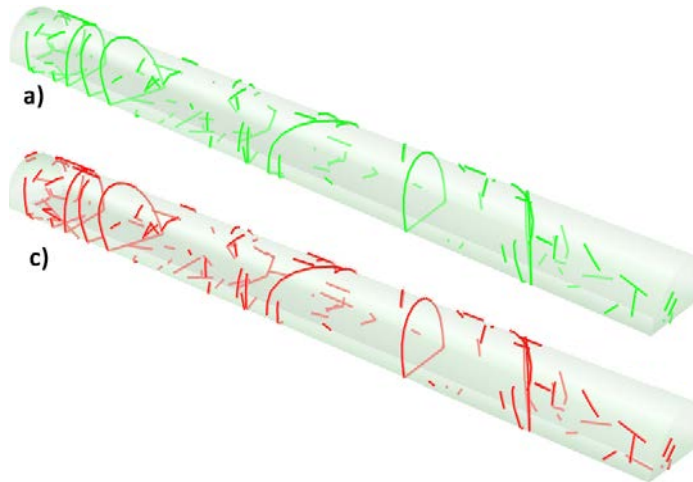


Figure 3.3: Comparison between a) original traces in NE Main Tunnel for case BM1-R4 and b) traces from model after conditioning. adapted from Figure 6-2 of Bym and Hermanson (2017).

Within the FracMan approach, a second step referred to as "connectivity conditioning," described in Section 3.1 of Bym and Hermanson (2017), is used to ensure that points where groundwater flows occur in underground openings correspond to fractures that have direct or network connections to the hydrogeological boundaries.

The third step in the FracMan approach is "hydraulic conditioning" to honour data from hydraulic tests in the underground openings (flows to tunnels and/or steady-state flows to boreholes during simulated hydraulic tests). This is accomplished by using a general-purpose model parameter estimation tool, PEST (Doherty, 2015), to adjust the hydraulic properties of a finite-element mesh representation of the DFN realization. PEST controls the search of the parameter space using multiple runs of a flow model (in this case Mafic which is part of the FracMan package). The mesh properties are adjusted until an adequate match to the specified set of inflows or hydraulic test results is obtained.

3.1.3. Predicting flows to open deposition holes

The main focus of both studies was verification of the conditional simulation methods, and testing their effectiveness for predicting flows to deposition holes for spent nuclear fuel, given the type of data that could be obtained from pilot holes and tunnels prior to boring the deposition holes.

In both cases, the DFN statistical model was assumed to be known *a priori*. The modelling teams began by using DFN models based on exactly the same statistical formulation as was used to generate the HypoSite "synthetic realities." Thus, this exercise did not include validation of the process of inference of a DFN statistical model. The implications of this in relation to a real repository situation are discussed briefly in Section 3.1.5.

Both teams tested the ability of their conditional simulations to predict steady-state inflows to deposition holes, but they differed in the types of data used for these predictions, and the number of realizations.

Bym and Hermanson (2017) only used data from the pilot boreholes for the deposition tunnels plus fracture trace data from the main tunnel in the HypoSite model, and they produced just one conditional realization. They concluded that there is very little match between the conditioned model and the deposition-hole inflows from their single realization (Figure 3.5). They suggested that data from much closer to the deposition holes would likely be needed to improve results. Such data could in fact be available, for example from structural geological mapping of the deposition tunnels and drilling of pilot holes for deposition holes. However prior to obtaining these additional data, these results by Bym and Hermanson suggest that possibilities to predict the locations of deposition holes with low inflow are limited.

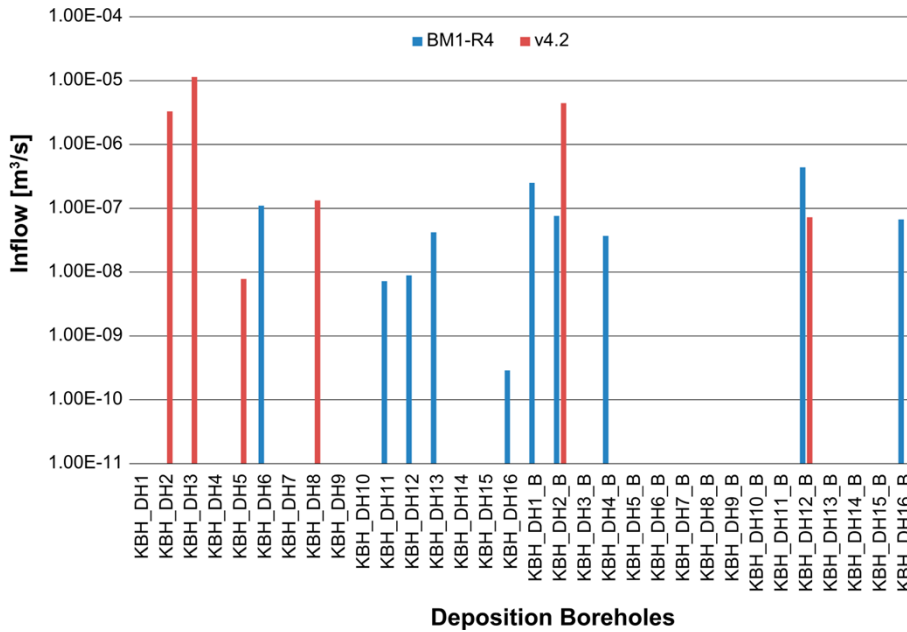


Figure 3.5: Comparison between "true" flows to deposition holes in the synthetic reality of HypoSite model BM1-R4 (in blue) and flows predicted by a single realization of a DFN model conditioned to geometric data from the main tunnel and flow data from pilot holes for the deposition tunnels (in red). From Figure 6-18 of Bym and Hermanson (2017).

With the ConnectFlow demonstration, Appleyard et al. (2017) incorporated additional information not used by Bym and Hermanson (2017), including geometric and inflow data from the pilot holes for the deposition holes, and they produced an ensemble of 10 conditional realizations.

They presented their results in terms of two stages of conditioning. When the model was conditioned only based on geometric data from the pilot holes, the predictions spanned a broad range, varying by up to four orders of magnitude for a given deposition hole (Figure 3.6). For most flowing holes, the synthetic "measured" inflows fell within the predicted range for the ensemble. However for five holes the "measured" inflow exceeded the maximum predicted value, including one hole (NNWB-5) that was predicted to be effectively dry in all realizations.

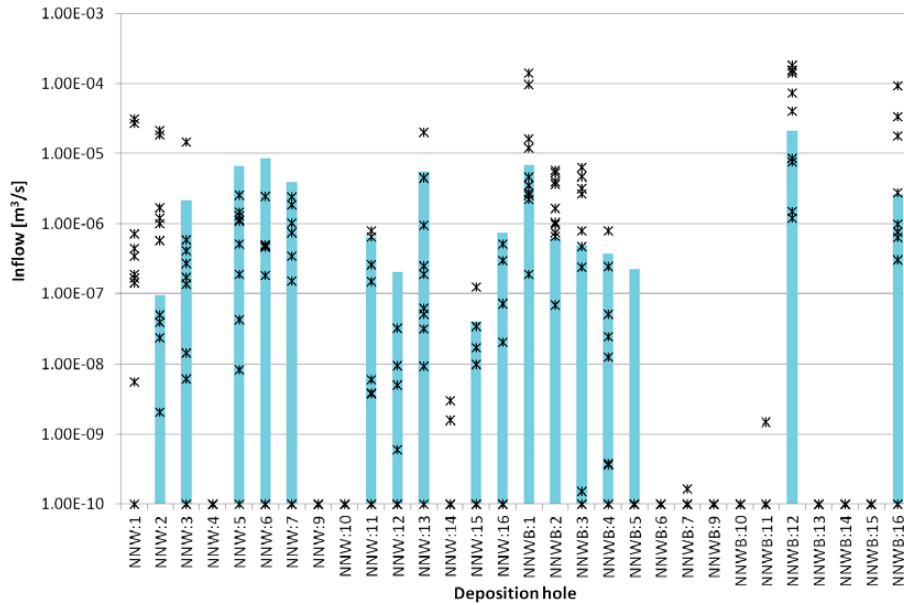


Figure 3.6: Comparison between "true" flows to deposition holes in the synthetic reality of HypoSite model BM1-R4 (blue bars) and flows predicted by ten realizations of a DFN model conditioned to geometric data (black X symbols). From Figure 4-2 of Appleyard et al. (2017).

After also conditioning to hydraulic measurements in the pilot holes for the deposition holes, the agreement between ensemble predictions and synthetic "measured" inflows was improved for many of the holes (Figure 3.7), though some discrepancies are still noticeable.

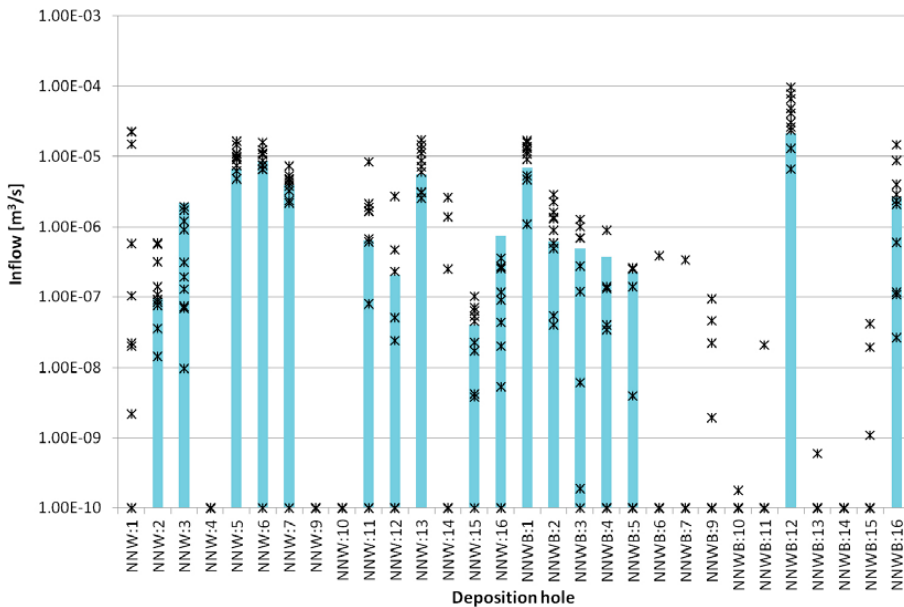


Figure 3.7: Comparison between "true" flows to deposition holes in the synthetic reality of HypoSite model BM1-R4 (blue bars) and flows predicted by ten realizations of a DFN model conditioned to both geometric and hydraulic data (black X symbols). From Figure 4-3 of Appleyard et al. (2017).

In considering these results, it is important to recall that both the synthetic "reality" (HypoSite model) and these conditional simulations are based on DFN models in which each fracture has homogeneous hydraulic properties. Greater discrepancies could be expected for a model in which fractures have heterogeneous properties, so simulated hydraulic measurements in a pilot hole could be strongly influenced by local properties of each fracture at its intersection with the pilot hole. This issue is not discussed by Appleyard et al. (2017) but it is considered in a separate study by Bym and Follin (2019), discussed in Section 3.3 of this review.

3.1.4. Predicting post-closure performance measures

Appleyard et al. (2017) go on to calculate two key performance measures for deposition holes after backfilling and closure of the hypothetical repository:

- Average flow-rate per unit length (U), and
- Flow-related transport resistance (F).

These are calculated both for the "true" HypoSite model (synthetic reality) and for the ensemble of ten conditional realizations.

They present results for several stages of conditioning based on geometric and hydraulic data that could be obtained at different stages of deposition-hole characterization. For safety assessment purposes, the most relevant stage is conditioning based on all geometric and hydraulic data that could be expected to be available after a deposition hole has been bored, as this reflects the information that would be available prior to the final decision as to whether to place a spent-fuel canister in the hole.

The results for U as shown in Figure 3.8 show that the "real" post-closure flows are generally within the range of predictions for the ensemble of conditional realizations, except for a few deposition holes that do not experience flow in the "real" case. Predictions may differ from "reality" by as much as three orders of magnitude. Thus the residual uncertainty is still quite high.

Notably, however, the prediction errors tend to be in the direction of higher values of U than occur in the synthetic reality. There are no deposition holes for which the "real" value of U exceeds the range predicted by the ensemble. Thus for safety-assessment purposes the predictions of the model appear to be conservative, at least for the idealized situation represented by the HypoSite model (hydraulically homogeneous fractures without channelling effects).

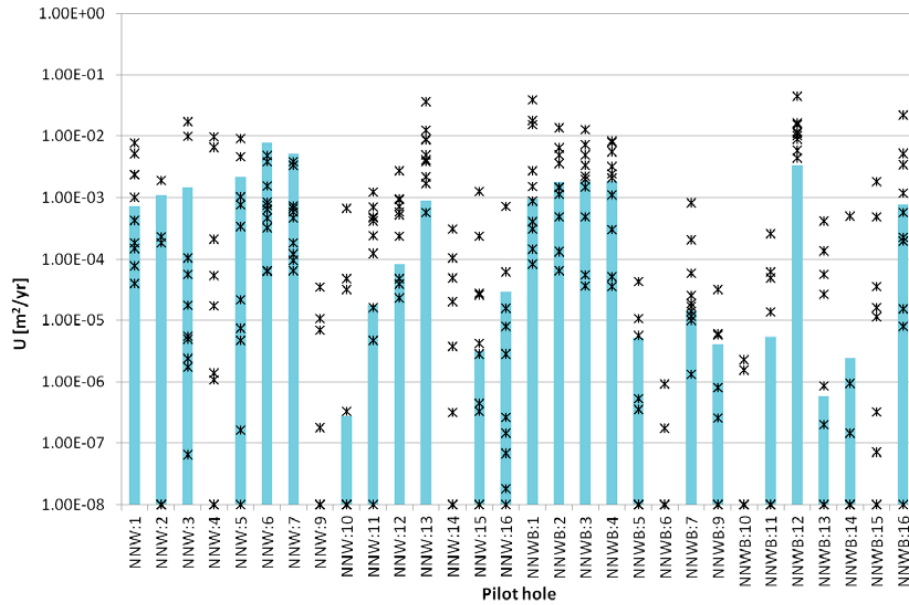


Figure 3.8: Comparison between "true" post-closure U values for deposition holes in the synthetic reality of HypoSite model BM1-R4 (blue bars) and U values predicted by ten realizations of a DFN model conditioned to both geometric and hydraulic data (black X symbols). Values less than or equal to 10^{-8} m²/yr are marked as 10^{-8} m²/yr. From Figure 4-15 of Appleyard et al. (2017).

The corresponding results for flow-related transport resistance F (Figure 3.9) show that the "real" post-closure F values again are generally within the range of predictions for the ensemble of conditional realizations, except for a few deposition holes that do not experience flow in the "real" case, and one hole where the "real" F is an order of magnitude lower than the lowest F predicted by a conditional simulation. Notably there are no flowing deposition holes for which the "real" value of F is lower than the range predicted by the ensemble. Thus again for safety-assessment purposes, the predictions of the model appear to be conservative.

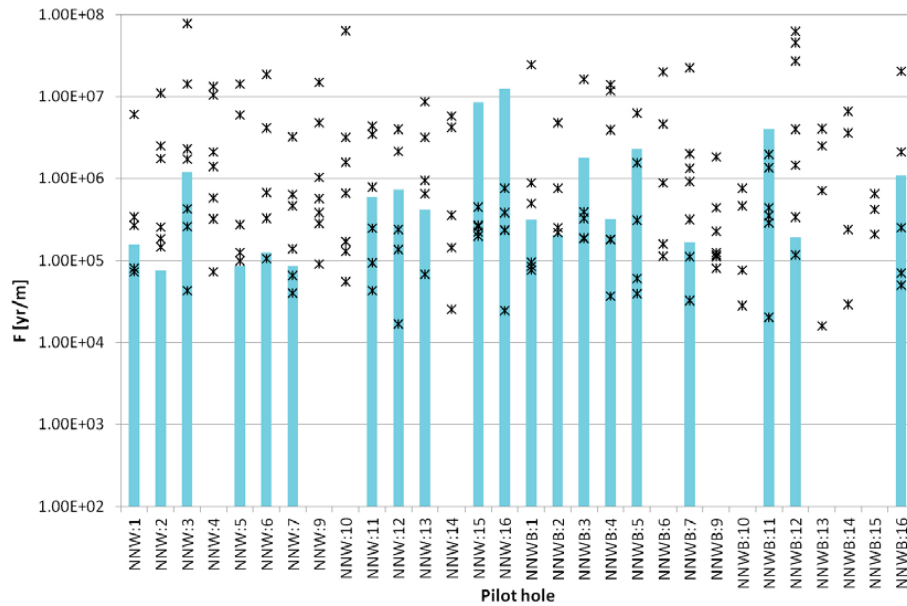


Figure 3.9: Comparison between "true" post-closure F values for deposition holes in the synthetic reality of HypoSite model BM1-R4 (blue bars) and F values predicted by ten realizations of a DFN model conditioned to both geometric and hydraulic data (black X symbols). Values greater than or equal to 10^8 yr/m are excluded. From Figure 4-18 of Appleyard et al. (2017).

Bym and Hermanson (2017) did not include prediction of post-closure flows to deposition holes, so their results do not give further information about the reliability of conditional DFN models to accurately predict these performance measures.

3.1.5. Discussion of results

The main focus of the DFN-R project was on development and demonstration of methods for conditional simulation of DFN statistical models with respect to the types of fracture observations that are expected in a repository situation. This exercise did not include validation of the process of inference of the DFN statistical model, but only conditional simulation for a synthetic reality in which the true statistical model was fully known to the modelling teams.

In a real repository situation, the DFN statistical model would need to be estimated from the same types of data used for conditioning here (mapping of fracture traces in underground openings and hydraulic measurements in boreholes), plus additional data from earlier investigations at the ground surface. This estimation process is subject to uncertainty both regarding the correctness of the chosen statistical representation (e.g. conceptual uncertainties regarding spatial organization of fractures, type of fracture size distributions, and variability of fracture hydraulic properties) as well as uncertainty in estimating the statistical parameters from underground exposures of limited extent.

More stringent validation of the DFN approach should be expected from SKB before the operating licence stage, to give confidence in the capability of these models to predict the key long-term measures (post-closure flows and transport resistances for deposition holes) that are important for safety assessment. The results of Appleyard

et al. (2017) demonstrate so far only that a conditional DFN model can predict these measures for the idealized situation represented by the synthetic "reality." A more complete validation should be expected to include prediction-outcome studies in which these models are applied to predict quantities that are then measured in the early stages of underground repository construction.

3.2. Coupling of models to hydraulic stresses

A third DFN-focused report focuses on coupling of models to hydraulic stresses, with an emphasis on shallow bedrock:

- SKB R-21-13. Exploratory integration of DFN models and 1D stress models with data from hydraulic tests for the shallow bedrock at the Forsmark site (Hartley, et al., 2021).

The principal aim is an integrated DFN description of shallow and deep bedrock at Forsmark, including the role of sheet joints in shallow bedrock. In past modelling by SKB for SR-Site this has been described in terms of a "shallow bedrock aquifer."

As Hartley et al. (2021) note, this was represented in the site descriptive model SDM-Site as "*a purely hypothetical structural model consisting of three parallel structures at 40 m, 80 m, and 120 m depth.*" They further note that low groundwater levels observed in wells drilled in the shallow system of fractures could only be matched if the anisotropy of the hydraulic conductivity of the equivalent continuum porous medium (ECPM) model was significantly modified by increasing the hydraulic conductivity anisotropy to be much greater in the horizontal than in the vertical direction.

The poor understanding of this shallow bedrock system stemmed in part from the tendency in earlier investigations to focus on the deeper bedrock. Most core-drilled holes Forsmark were drilled with a telescopic drilling technique in which the uppermost 100 m was drilled by percussion methods, then cased before starting to obtain drill cores from greater depths.

More recently, fracture data have been acquired from shallower sections of KFM13 – KFM24, which allow construction of an integrated model for both shallow and deeper bedrock. This includes data on very shallow, subhorizontal fractures that are interpreted as classic sheet joints produced by changes in vertical stress during past glaciations and deglaciations, as well as deeper features that may be splays of a gently dipping deformation zone, ZFMA2.

3.2.1. Update of DFN model

The work by Hartley et al. (2021) is aimed at updating the DFN descriptive model for the shallow bedrock, with a particular focus on taking into account the influence of stress on transmissivity of fractures and deformation zones. This work is focused mainly on the vicinity of the spent-fuel repository (Figure 3.10) but has some overlap with the area modelled to assessments of the low- and intermediate-level waste facility known as the SFR (Figure 3.11).

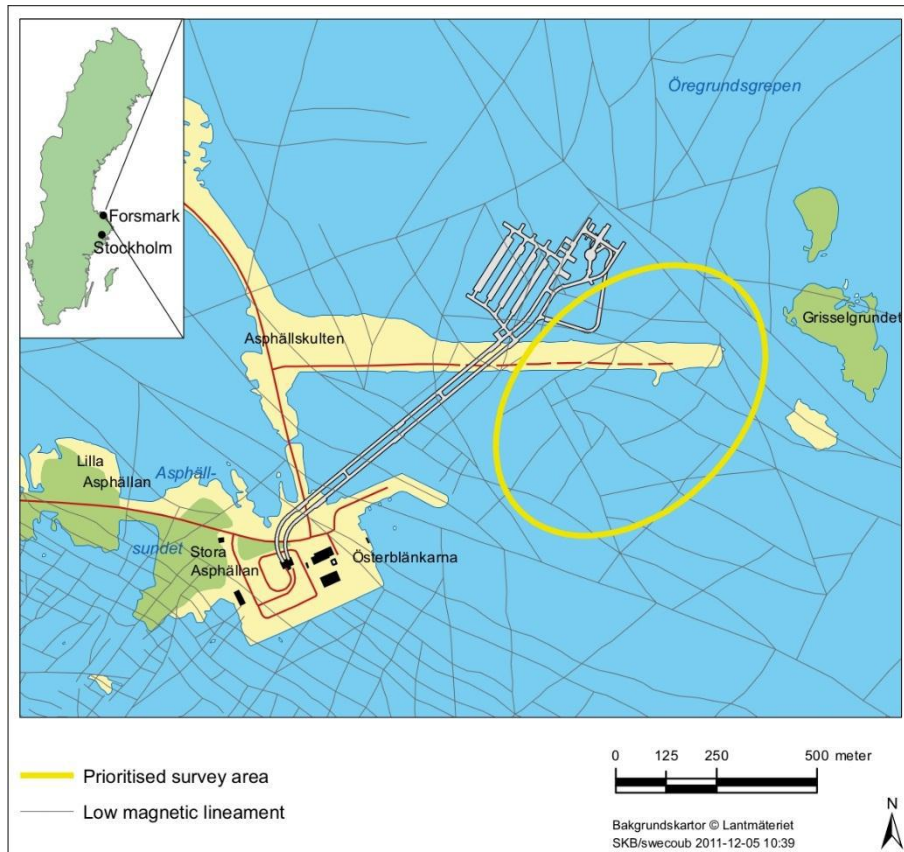


Figure 3.11: Map of the Forsmark-SFR area showing the location of the existing SFR and the area that was prioritized for an extension of this facility. From Figure 1-1 of SKB-R-11-10.

The update of the DFN model for the spent-fuel repository at Forsmark is comprehensive, including a re-analysis of fracture orientation, size, and intensity. A new database for fracture conceptualization and modelling, named FORSIDE and implemented in PostgreSQL, was developed as part of the work.

This analysis uses the same fracture domains as in SDM-Site (Geo-DFN model F2.2 developed by Fox et al. 2007), except that the domain FFM02 is split into FFM02L above an elevation of -30 m and FFM02U below (Figure 3.12). A model for the sheet joints in the upper domain FFM02U is developed based in part on geological mapping in the inlet channel during construction of the Forsmark reactor plant in 1979, together with borehole data from more recent investigations. Three variants of this model are developed:

1. Log-normal size distribution based on the best fit to the 1979 inlet mapping data;
2. Power-law size distribution fitted to the 1979 inlet mapping data; and
3. Log-normal size distribution based on the 1979 inlet mapping data but treating the trace-length data as effective radii of the sheet joints, resulting in larger sheet joints.

Figure 3.13 shows cross-sections through a realization of the fracture population based on the first of these variants.

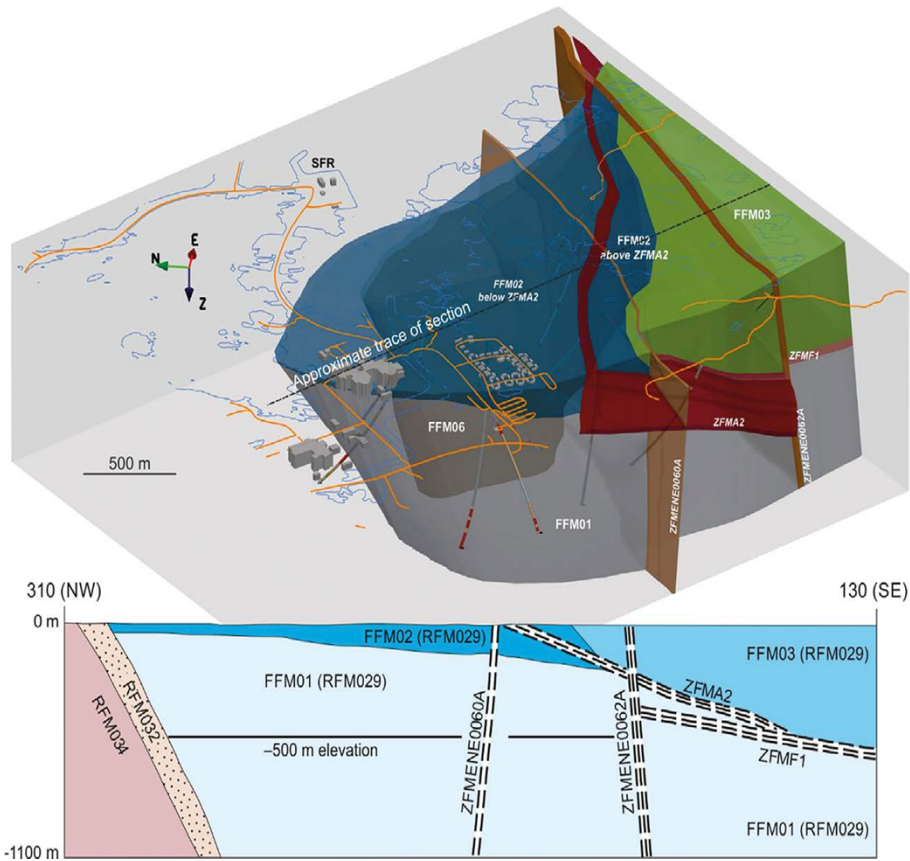


Figure 3.12: Facility-scale 3D geometric model for fracture domains FFM01, FFM02, FFM03 and FFM06 in the north–western part of the Forsmark tectonic lens, viewed towards the east–north–east (at top); Simplified NW–SE trending profile showing the same fracture domains (at bottom). From Figure 2-7 of Hartley et al. (2021).

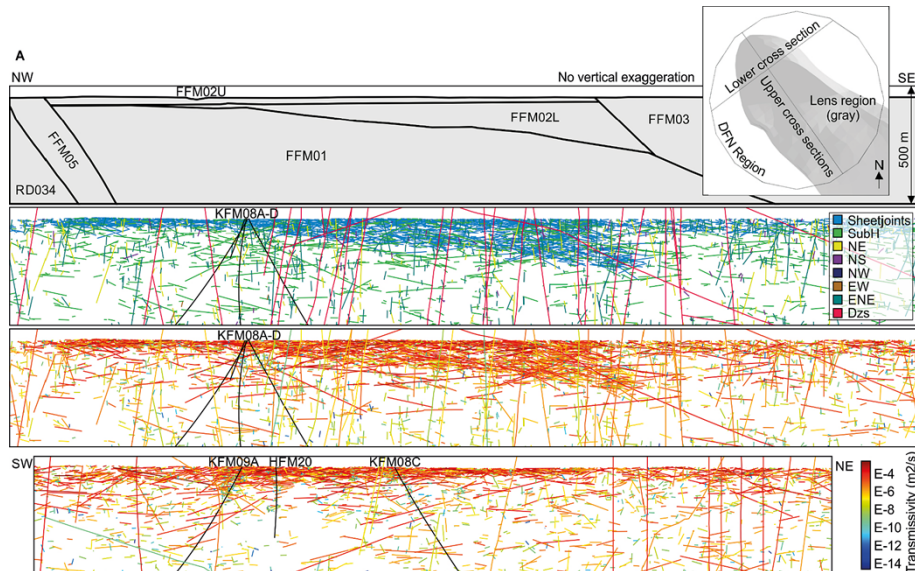


Figure 3.13: Cross-sections across the DFN region for the Variant 1 model showing fracture traces coloured by set and transmissivity. Sheet joint model based on 1979 mapping of Forsmark reactor inlet channel. From Figure 3-21 of Hartley et al. (2021).

3.2.2. Accounting for effects of rock stress on hydraulic aperture

A key feature of this new DFN model is that fracture transmissivities are related to rock stresses. The general approach was developed earlier in a model of the Olkiluoto site in Finland (Hartley et al., 2016) and closely follows the same methodology. The effects of rock stresses on fracture hydraulic aperture e_h , which is related to transmissivity by the cubic law:

$$T = \frac{\rho g e_h^3}{12\mu}$$

where ρ is fluid density and μ is dynamic viscosity, are modelled by a hyperbolic model for aperture closure in response to increasing effective normal stress:

$$e_h = e_{hr} + \frac{1}{f} \left(\frac{A e_{m0}}{1 + \frac{9\sigma'_n}{B}} + e_s \right)$$

Here A and B are empirical parameters, e_{m0} is the unstressed fracture aperture, σ'_n is the effective normal stress (normal stress minus pore pressure) acting across the fracture, f is a factor related to fracture surface roughness, and e_s is the shear slip induced fracture dilation. The last component e_s is ignored in this application, so in practice this becomes:

$$e_h = e_{hr} + \frac{1}{f} \left(\frac{A e_{m0}}{1 + \frac{9\sigma'_n}{B}} \right)$$

The authors do not define e_{hr} but this appears to be a component of the residual hydraulic aperture that exists for the situation of effective stress.

The mechanical aperture is assumed to be correlated to fracture size according to a power-law scaling relation:

$$e_m = aL^b$$

with b around 0.5. The authors do not state whether e_m in this equation (given as Equation 4-1 in the text) is the same as e_{m0} in the previous equation (given as Equation 4-6 in the text) in the text, but by comparison with the previous work by Hartley et al. (2016), this appears to be the case.

The effective normal stress σ'_n is calculated from a 1D stress model developed for SDM-Site inside fracture domains FFM02/FFM01/FFM06 and for FFM03 outside the Forsmark tectonic lens. This stress model is expressed in terms of expressions for the principal stress components (major horizontal stress σ_H , minor horizontal stress σ_h , and vertical stress σ_v) as linear functions of elevation z , for a given domain. In all domains and at all depths in this model, σ_v is the minimum principal stress and the major horizontal stress σ_H is oriented NW-SE (azimuth 145°).

For a given fracture within the DFN model, the effective normal stress σ'_n is evaluated by calculating the component of this stress model in the direction normal to the fracture plane, and subtracting the groundwater water pressure (assumed hydrostatic).

Effects of rock stresses on the effective transmissivity of deformation zones at depth are accounted for in an analogous fashion. A corresponding hyperbolic model for

decrease in hydraulic aperture as a function of the σ'_n is assumed to apply at each point where the zone transmissivity has been measured via an intersecting borehole. The measured transmissivity $T(z)$ for an intersection at a given depth z is corrected for the effect of stress σ'_n to yield a depth-corrected estimate of what the transmissivity would be if σ'_n were equal to zero (i.e. the expected value of $T(z)$ for $z = 0$).

These depth-corrected estimates of deformation zone $T(z=0)$ at borehole intersections are then used as the basis for calculating depth-corrected $T(z=0)$ for other points on the same deformation zone (using an inverse distance squared weighting scheme). Finally these interpolated values are converted to T values for the actual depths.

The result is a model of the deformation zones in which the transmissivity of a given zone generally decreases smoothly with depth, while also honouring measured values at borehole intersections so that some lateral heterogeneity is allowed (Figure 3.14).

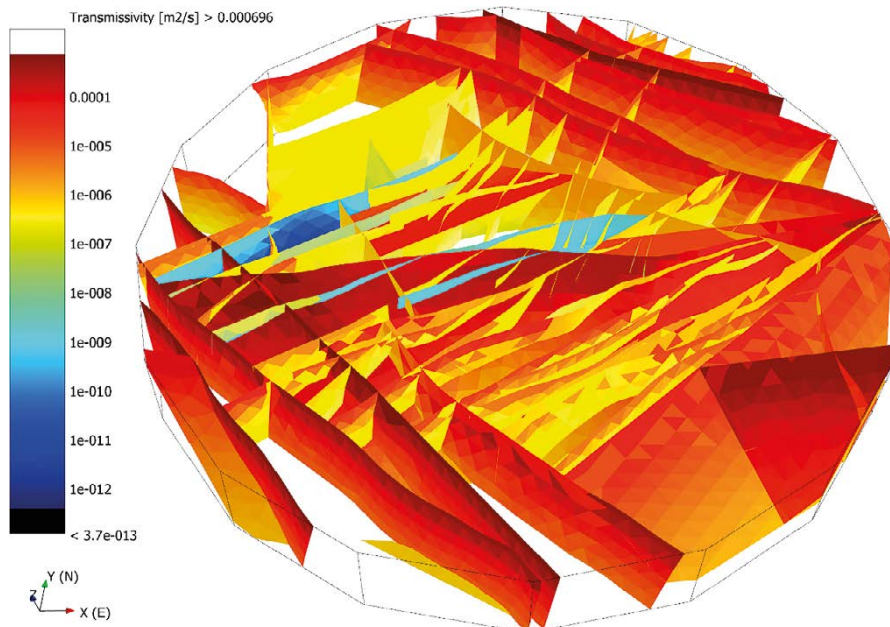


Figure 3.14: 3D view of the deformation zone surfaces coloured by transmissivity within the DFN facility-scale model down to -440 m elevation, after accounting for estimated effects of stress with depth and interpolating between borehole measurements. From Figure 4-3 of Hartley et al. (2021).

The idea that transmissivity decreases with depth in most deformation zones at Forsmark has been a feature of the hydrogeological site-descriptive model at least since the surface-based site investigation stage, when Follin et al. (2007) proposed that the transmissivity of all deformation zones could be assigned a depth-dependent transmissivity of the form:

$$T(z) = T_0 \cdot 10^{z/k}$$

where T_0 is the transmissivity at $z = 0$, and k is a constant which Follin et al. (2007) estimated as 232.5 m, resulting in roughly a half-order-of-magnitude decrease in transmissivity per 100 m depth.

The approach of Hartley et al. (2021) provides a mechanistic explanation for the inferred decrease in transmissivity of deformation zones with depth. An implicit assumption of this approach is that the transmissivity of each deformation zone is controlled primarily by fractures with orientations parallel to the deformation zone. In terms of the fault zone architectural styles proposed by Caine et al. (1996), this type of behaviour could be expected for single-fracture faults.

The approach may be overly simplistic for other fault-zone styles identified by Caine et al. (1996), including distributed deformation zones in which flow is carried by a dense network of fractures of variable orientation, or localized deformation zones in which flow may be primarily through breccia. In such cases, the influence of the stress field net transmissivity of the feature may be more complicated than the simple hyperbolic-closure model considered by Hartley et al. (2021).

The methodological developments of Hartley et al. (2021), accounting for depth-dependent stress effects both in the stochastic DFN model and in deterministic deformation zones, should enable more realistic treatment of the near-surface rock, and limit need for artificial division of the DFN model into "depth zones" in future site modelling. However further assessment of the model for transmissivity of deformation zones at depth is recommended, to take into account the likelihood that zones with different architecture will have different responses to stress.

3.2.3. Preliminary applications of new model

Hartley et al. (2021) applied this updated hydrogeological description of the major deformation zones and bedrock fracture system to simulate an interference test that was previously conducted in a shallow percussion-drilled borehole, HFM43, located near the centre of the modelled domain. After calibrating on single-hole hydraulic tests, the DFN model was upscaled to an ECPM (continuum) representation to calculate drawdowns in observation wells.

The results (Figure 3.15) show a reasonable degree of success in matching the magnitudes of drawdowns measured in early time (0 to 2 days) and at the end of the interference test (21 days). However, the model does not reproduce the variability of response seen at different depth intervals in a given borehole. Hartley et al. (2021) also note that the model does not reproduce the discrete nature of measured responses, with boreholes in some areas unaffected by the pumping in HFM43. They suggest that this may be a consequence of the ECPM representation which is more continuously connected than a DFN representation.

Hartley et al. (2021) also explored alternative methods for upscaling from a DFN to an ECPM representation. Their findings confirm results of earlier studies, including within SSM's own review of SR-PSU (Geier, 2017), which concluded that geometrical upscaling methods tend to give high estimates of effective hydraulic conductivity relative to what would be obtained by explicit DFN network calculations.

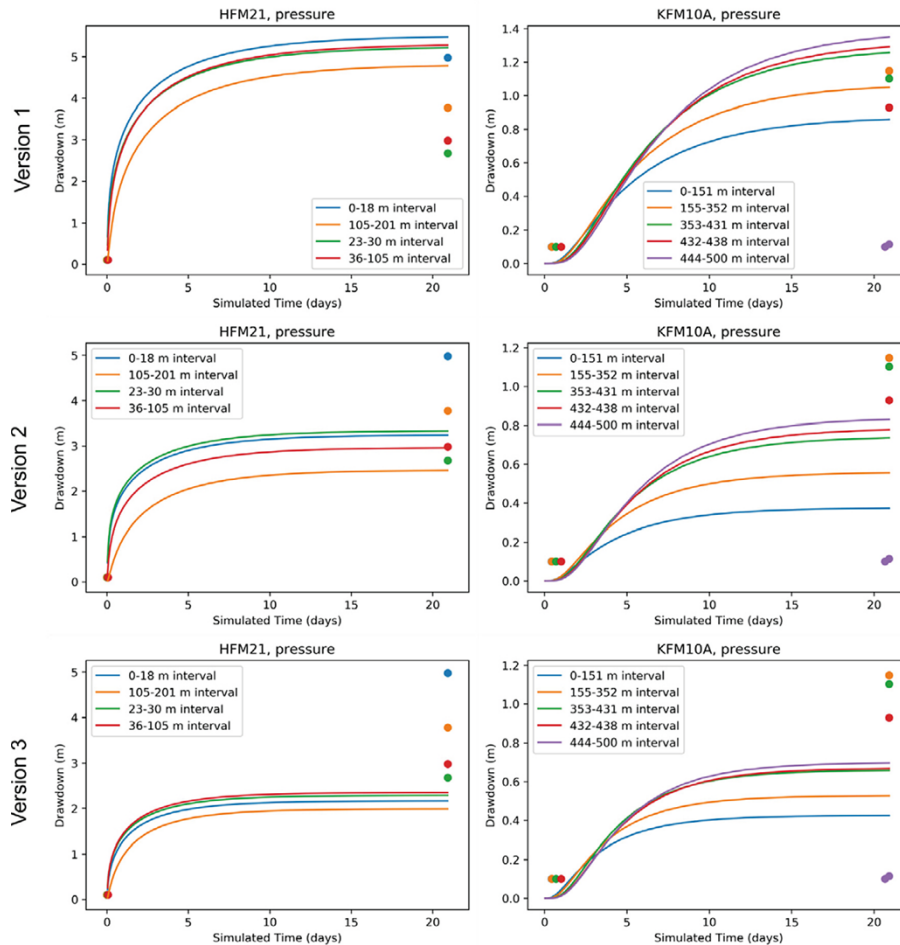


Figure 3.15: Graphs showing the flow responses for the actual interference test (dots) and three different fracture variants (lines) for a borehole close (< 200 m) to the pumping hole and far (> 1 500 m) from the pumping hole (HFM21 and KFM10A respectively). From Figure 4-23 of Hartley et al. (2021).

3.3. Effects of fracture heterogeneity on transport

A fourth DFN report investigates the effects of channelling in DFN models in conjunction with calibration to borehole data:

- SKB R-19-24. A numerical study of channelling in heterogeneous versus calibrated homogeneous DFN realisations (Bym and Follin, 2019).

The objective of this study is clearly stated by the authors: "*to evaluate whether a flow-calibrated DFN model, where each fracture is assumed hydraulically homogenous, can reproduce the particle tracking behaviour of a DFN model, where each fracture is hydraulically heterogeneous.*"

Like the DFN-R study discussed in Section 3.1, this investigation was also based on synthetic data, using a known DFN geometry which is treated as representing "reality." However in this case the synthetic data are based on a DFN model in which each fracture has heterogeneous hydraulic properties.

3.3.1. Numerical experimental approach

The main part of the study by Bym and Follin (2019) is in the form of a numerical experiment with the following steps:

1. A DFN realisation with heterogeneous fracture properties is generated, referred to as the "Reality Realisation".
2. A pumping test is simulated in the Reality Realisation, mimicking the performance of measurements with the Posiva Flow Log (PFL) tool.
3. A DFN realisation with identical geometry to the Reality Realisation, but with homogeneous hydraulic properties within each fracture, is calibrated with respect to the inflows in the simulated PFL measurements.
4. Particle tracking is performed in this calibrated, homogeneous-fracture model, and compared with particle tracking results for the Reality Realisation.

It may be noted that the calibration in Step 3, using a "known" network geometry, is an artificial situation relative to the situation for a real-world calibration, where the geometry of the network as well as the hydraulic properties of the fractures would be unknown. Thus this represents a numerical experiment to explore just one aspect of the network calibration problem, with constraints on other sources of uncertainty that would exist in a real-world calibration.

This procedure was carried out for ten such realizations of the fracture network geometry, within a 400 m x 400 m x 800 m deep domain, with the pumping test and PFL measurements being in a vertical borehole centred in the domain (Figure 3-16).

The same DFN statistical model was used for all realizations, with three sets of fractures in nominally orthogonal orientations: subvertical with NNE strike (strongest set), subhorizontal (secondary set), and subvertical with WNW strike (weakest set). This results in an anisotropic, sparsely connected network.

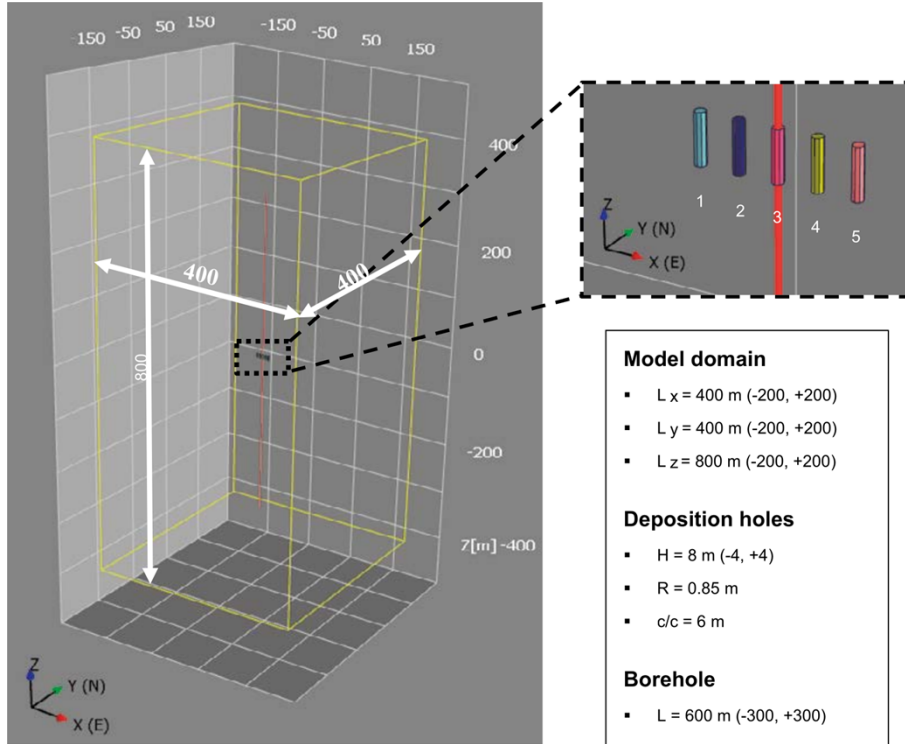


Figure 3.16: Model domain used for simulation of realizations of PFL measurements in a vertical borehole and particle-tracking from five deposition holes. From Figure 4-1 of Bym and Follin (2019).

Models for intra-fracture heterogeneity

For each realization of the fracture network geometry, four different models of heterogeneity for hydraulic properties within each fracture plane were considered, based on two patterns referred to as A and B, with two variants in each case, with transmissivity either correlated or uncorrelated to the size of the fractures by a relationship which can be written as:

$$\log T = \delta + \log(1.6 \times 10^{-9} \cdot r_e^{0.8})$$

in the correlated case, or:

$$\log T = \delta - 8$$

in the uncorrelated case, where δ is the Gaussian random variable from the simulated pattern (either A or B) as mapped to a given point in a fracture plane, and r_e is the equivalent radius of the fracture.

Bym and Follin (2019) do not state explicitly where they give these expressions (in slightly different form in Table 4-2), so unfortunately the reader is left to guess whether the logarithm is base 10 or natural (base e), and what are the units of T and r_e . Assuming that the logarithm is base 10 and that T and r_e are in units of m^2/s and m , respectively, for the uncorrelated case this results in fractures that have a mean transmissivity of $10^{-8} \text{ m}^2/\text{s}$. For the correlated case, fractures with $r_e \approx 10 \text{ m}$ have a mean transmissivity of $10^{-8} \text{ m}^2/\text{s}$, while larger or smaller fractures will have larger or smaller mean transmissivity, respectively.

Both patterns A and B were generated by the same Gaussian geostatistical model with an anisotropic covariance within a given fracture plane. For pattern B the field of Pattern A was modified by a numerical transformation suggested by Zinn and Harvey (2003). Pattern A yields relatively large areas of connected high transmissivity with isolated patches of low transmissivity, while Pattern B yields larger connected areas of low transmissivity with isolated patches of high transmissivity, resulting in stronger flow channelling (Figure 3.17).

The patterns were mapped onto each fracture independently so the local pattern of heterogeneity is not contiguous between fractures. This means that there was no tendency for persistent channels to form between fractures. The authors do not claim empirical or theoretical support for either pattern as representing realistic patterns of fracture heterogeneity, so both patterns can be viewed as speculative.

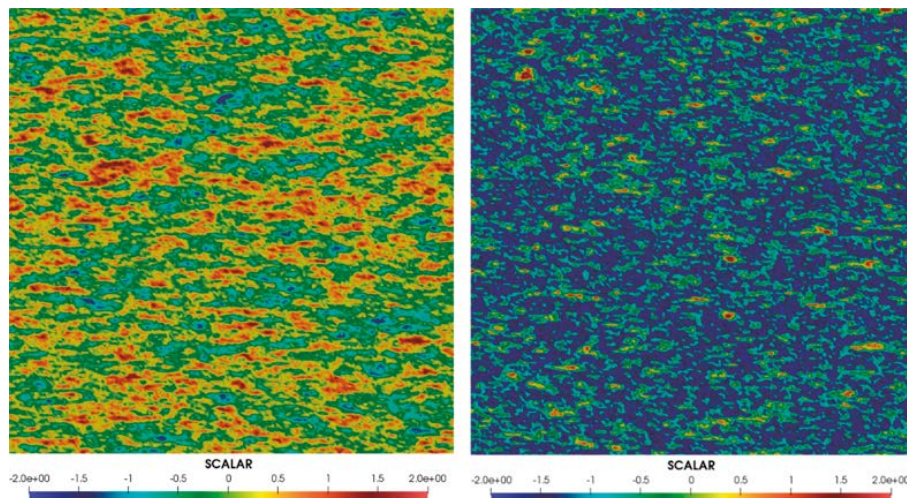


Figure 3.17: Visualisation Pattern A (left) and Pattern B (right) for heterogeneity of the variate δ within a given fracture. From Figure 4-2 of Bym and Follin (2019).

Calibration of homogeneous models to simulated PFL tests

The study used 40 different calculation cases to simulate fluid flow. This involved 10 different DFN geometric realizations, each with four variations of heterogeneous transmissivity within the fractures. In each of these 40 calculation cases, the following procedure was performed:

- PFL measurements were simulated in the heterogeneous-fracture model by calculating inflows for a situation of steady-state drawdown in the borehole.
- A DFN model with identical network geometry, but constrained to have homogeneous properties within each fracture, was then calibrated to attempt to match the simulated PFL measurements from the heterogeneous-fracture case.

In both of these steps, simulated inflows to the borehole were calculated by the finite-element method flow solver, Mafic. The calibration was carried out using the parameter-estimation tool PEST (Doherty, 2015).

Two different algorithms within PEST were used, resulting in a total of 80 different calibrated models with homogeneous fractures. Of these calibrated models, 23 of the calibrations (29%) were of poor quality and were not used for further analysis. The

most successful calibrations tended to be for the cases in which the corresponding heterogeneous-fracture model ("reality realisation") included a correlation of transmissivity to size.

Particle tracking

Finally, particle-tracking for sources located at the five deposition-hole locations was performed in each calibrated homogeneous model, and compared with results of particle-tracking in the heterogeneous "reality realisation." This particle-tracking was performed in a flow field with steady-state boundary conditions to impose an upward head gradient of 0.5% (0.005 m head decrease per m).

Particle-tracking results were summarized both in terms of the transport resistance F for the fastest-arriving particle from each deposition hole, and the geometric mean value of F_{mean} for the ensemble of particles.

3.3.2. Results

The results as summarized in Figure 3.18 show that the calibrated homogeneous models tend to produce higher values of F_{mean} than the corresponding homogeneous "reality realisation." With exception of the case of Pattern A, combined with a correlation of transmissivity to fracture size ("Pat_A+size"), results for most realisations plot above the 1:1 line, indicating that the calibrated homogeneous models produce a non-conservative model prediction relative to "reality."

Bym and Follin (2019) note that results for the "Pat_A+size" case show both conservative and non-conservative values relative to "reality." The vertical axis for this case (upper left plot in Figure 3.18) only has one numerical value so the scale is somewhat unclear. However from the tick marks on this axis, it appears that the highest and lowest values are separated by less than one order of magnitude.

They conclude that the homogeneous DFN model is generally non-conservative for predicting transport, even after calibration to PFL measurements.

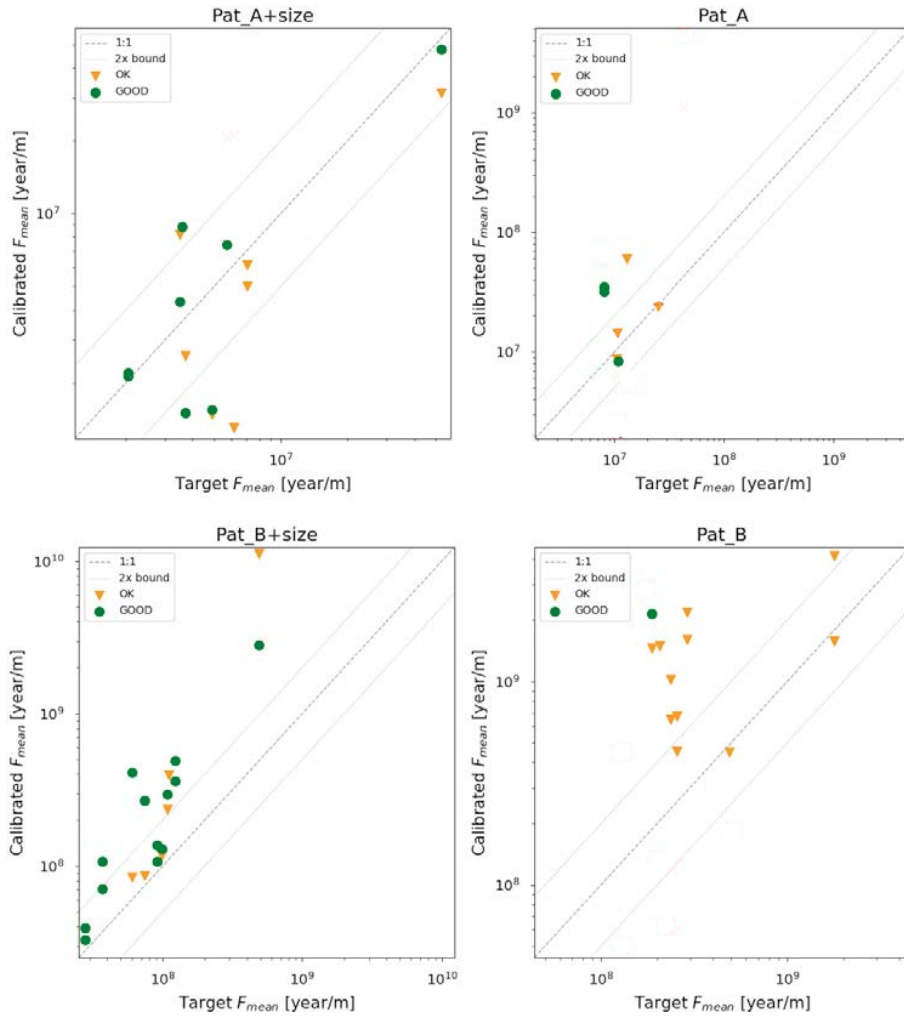


Figure 3.18: Cross plots comparing geometric mean transport resistance (F_{mean}) for calibrated models with homogeneous fractures (y-axis) versus that for the corresponding "reality realisation" with heterogeneous fractures (x-axis). Symbol colours indicate the quality of the calibration (green for "good" and yellow for "OK"). Separate plots are given for Pattern A and Pattern B, with and without a correlation to fracture size (radius). Adapted from Figure 4-12 of Bym and Follin (2019), deleting points for bad-quality calibrations which the authors note are not meaningful for this type of comparison.

3.3.3. Comparison with previous SKB studies

The main result of Bym and Follin (2019) seems to contradict earlier work commissioned by SKB. Painter and Cvetkovic (2001) previously investigated the relative role of intra- vs. between-fracture variability, and concluded that intra-fracture aperture variability contributes little to field-scale transport because it is overwhelmed by the much larger fracture-to-fracture variability. Subsequent work by Painter (2006) found that intra-fracture heterogeneity can have some effect, but only when the internal variability is at least as great as the variability between fractures.

The differing conclusions between the current study and the previous work may be due in part to differences in the representations of intra-fracture heterogeneity. The model of Painter (2006) assumes isotropic covariance of transmissivity within a given fracture, rather than anisotropic. This reduces the likelihood of a preferred direction of channelling within a given fracture. The simulation method employed by Painter was a conventional multi-normal function with an exponentially decaying autocorrelation. Thus this was most comparable to an isotropic version of Pattern A, without considering the type of transformation used for Pattern B, which produces stronger flow channelling.

Painter (2006) speculated that more complicated models with improved connectivity between large-aperture regions could lead to greater influence of channels on the network. This speculation seems to be borne out by the results of Bym and Follin (2019) particularly for the most strongly channelled case. More pronounced channelling, for example with persistent, self-reinforcing channels between fractures that might be formed by flow combined with mineral precipitation/dissolution, could conceivably lead to fracture heterogeneity having even stronger effects for network-scale transport.

Another difference between the previous work of Painter (2006) and this recent work by Bym and Follin (2019) is that the latter accounts for the possibility of errors that might occur in calibrating a homogeneous-fracture model to PFL measurements in a system of heterogeneous fractures. While the problem of calibrating DFN models to such data is a problem that exists in reality, it can be expected to add to the discrepancy between calibrated models and the synthetic "reality" considered here. *A priori* the discrepancies resulting from this step might be expected to be "neutrally" random with respect to flow-related performance measures for safety. The finding that calibration of a homogeneous-fracture model to flow data from a channelized fracture system could lead to non-conservative results suggests that this issue needs further consideration within SKB's overall methodology for DFN modelling.

3.4. Overall DFN Methodology

Applications of DFN models in SKB's repository siting and safety assessment programs over the past 40 years have tended to use differing terminology and approaches to data analysis, depending on different stages in development of software tools and concepts by the different research teams and consultants involved. Over the same time period, the DFN approach has gradually gained more importance within SKB's program, forming the common framework for quantitative description of bedrock geology, rock mechanics, hydrogeology, hydrogeochemistry and solute transport.

The report considered here is the following:

- SKB R-20-11. Methodology for discrete fracture network modelling of the Forsmark site. Part 1 – concepts, data and interpretation methods (Selroos et al., 2022).

This is the first volume of what is intended as a two-volume handbook for the modelling concepts, data analysis, and numerical techniques applied in modelling

naturally fractured crystalline rocks such as found at Forsmark. This first volume documents conceptual frameworks and analysis techniques for interpreting site data and constructing quantitative descriptions of fracture systems. The second volume (not yet published) is planned to provide practical guidance and methods for numerical modelling of fracture systems.

This first volume is mainly a review and compilation of results from past research and theoretical work, rather than current research. As such, it is not reviewed in any substantial depth here, as the main focus of this review is on SKB's recent research related to hydrogeology.

However some notable aspects of this report can be highlighted:

- It sets out for the first time (in Chapter 2), an outline of how DFN models are expected to be utilised during the construction and operational phase of a spent nuclear fuel repository, including an illustrative timeline of how DFN models could evolve during the construction process.
- It presents a coherent summary of typical DFN workflows (Chapter 3), starting with geometrical analysis, followed by development of more specialized DFN models for flow and transport, and prediction-outcome modelling as a means of building confidence in the reliability of the models and their fitness for purpose.
- Subsequent chapters (5 through 9) present a clear nomenclature and general procedures for the typical stages of DFN analysis, starting with a summary of methods for describing spatial variability, and proceeding on through the typical statistical methods in use for representing the geometric, flow, transport, and rock mechanics properties of fractures.
- A brief section titled "Beyond the fracture density distribution" (Section 6.3.5) points toward emerging concepts of fracture network architecture, including geomechanically-based models for fracture genesis and propagation (some of which is repeated in Section 7.1).
- Section 6.4.4, titled "Building the DFN models for a site," includes recommendations that could form the beginning of a quality-assurance program for the process of DFN analysis, including the need to document subjective decisions made at various stages of the process.

The report includes (in Chapter 4) an abbreviated summary of the geological site descriptive model for Forsmark, which contrasts with the otherwise mostly generic description of the rest of this report. This serves as a basis for occasional reference to site-specific characteristics of the fracture system at Forsmark.

From SSM's regulatory perspective, this document will be a useful point of reference for following SKB's work on DFN model development and adaptation during the construction and operational licensing of the spent nuclear fuel repository at Forsmark. While many parts of the document are still discursive rather than precise in offering prescriptions for future analyses, this report can be seen as an important step in bringing DFN methodology into the type of framework that will be necessary for quality assurance in the context of a real repository, as opposed to research situations.

One important thing missing from this report is any significant discussion of alternative concepts for flow and transport in sparsely fractured rock, outside of the

DFN approach. In particular, the sparse channel network (SCN) concept is given only cursory discussion in the introductory section, with reference to Dessirier et al. (2018), where it is discussed only briefly before being dismissed as a "process-specific" approach. No reference is given to work by Black et al. (2017) or Black and Barker (2018) who pointed out the insufficiency of DFN models – even those incorporating channelling within the DFN framework – to explain anomalous flow and transport behaviour observed in in-situ experiments.

The SCN concept points toward a more sparsely-connected system than can be reproduced even by channelised DFN models that are built up by following the DFN procedures described in this report. For a safety assessment, the SCN concept can be favourable in some respects as it leads to predictions of fewer deposition holes with significant flow and potential for transport to the biosphere. But it also leads to a prediction of more "dry" deposition holes that might require much longer time scales to resaturate, which means that the bentonite buffer might still be dry when exposed to peak heat generation by the spent-fuel canisters. The consequences of having many more "dry" holes have not been addressed directly in past safety assessments, so this is an aspect that may deserve consideration.

On a more minor level, the report is highly self-referential (for example, 32 references to work by one of the co-authors, and 22 references to work by another co-author). While these authors have certainly done significant work in the field of DFN theory, this imbalance reduces confidence in the degree to which alternative DFN approaches and alternative conceptual models such as the SCN concept have been taken into account.

4. Near-field modelling for SR-PSU

The last major topic considered in this review is the near-field modelling for the safety assessment SR-PSU (PSAR):

- SKB R-19-20. Modelling of the near-field hydrogeology – Report for the safety assessment SR-PSU (PSAR). Abarca et al. (2019).

This work concerns the future hydrogeological conditions in the near-field of the existing low- and intermediate-level waste facility known as SFR (referred to as SFR 1), and a planned extension (referred to as SFR 3). This is an extension of the analysis previously carried out as part of the long-term safety assessment for the SFR extension application (Abarca et al. 2013 & 2014).

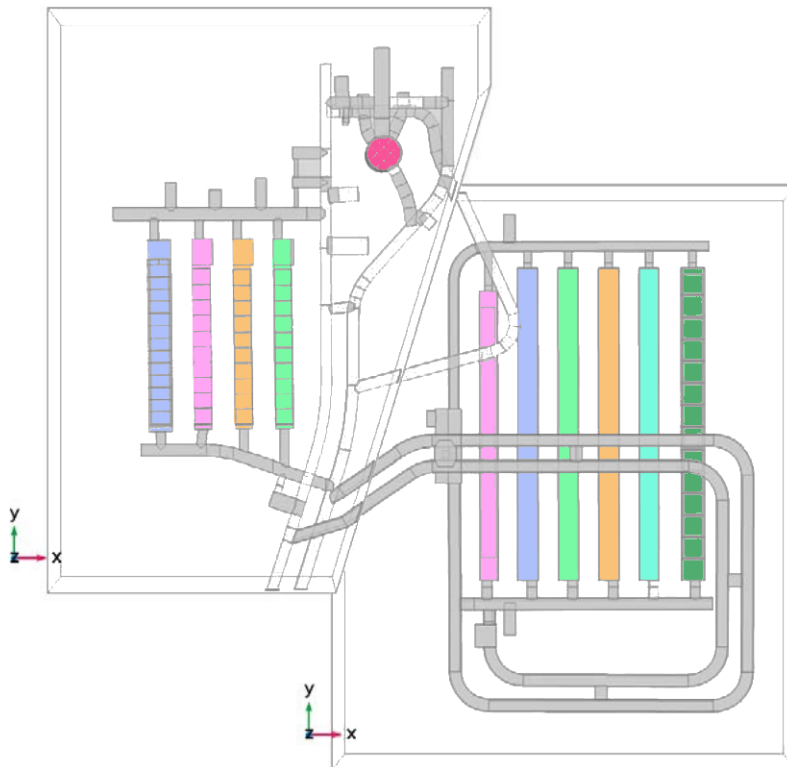


Figure 4.1: Plan view of vaults in the SFR 1 (left) and the proposed extension SFR 3. Within the SFR 1, the vaults in order from left to right are 1BMA (blue), 1BLA (pink), 1BTF (orange), 2 BTF (pale green) and the Silo (magenta). In the SFR 3 area the vaults are BRT (pink), 2BLA (blue), 3BLA (pale green), 4 BLA (orange), 5BLA (cyan), and 2BMA (dark green). Adapted from Figure 3-1 of Abarca et al. (2019).

Both this recent work and the previous analyses use results of regional hydrogeological modelling by Odén et al. (2013) as the basis for hydraulic boundary conditions. Values of pressure calculated by the regional-scale model are extracted for points along the boundary of the repository-scale model, and then used as prescribed-pressure boundary conditions in the latter model. The equivalent hydraulic conductivity field for the bedrock is also taken from the regional-scale models.

The main objectives of the original repository-scale model (Abarca et al., 2013) were to estimate groundwater flow rates within the repository, and to develop a

system understanding focusing on the effects of barrier degradation, closure alternatives, and permafrost. More detailed vault-scale models (Abarca et al., 2014) were used to address specific questions concerning the effects of concrete degradation of the 1BMA structure and transport of solutes around the Silo.

4.1. Updates in model geometry and calculation cases

The work of Abarca et al. (2019) is an update of the earlier work, mainly to account for changes in the design geometry of the SFR 3 including:

- Removal of the separate ramp for transport of reactor pressure vessels,
- Larger radius for the main ramp,
- Mirror-reversal of the direction of the vaults, and
- Modifications in the dimensions of the vaults, especially BRT and 2BMA.

The updated model also takes into account technical developments relating to the concrete structures in the SFR 1 including:

- Reinforcement walls for the concrete structures in 1BMA,
- A foundation of grouted gravel in 1BMA,
- A gas-venting system in 1BMA and 2BMA
- Modifications in the dimensions of the vaults, especially BRT and 2BMA.

Aside from these changes, the main part of the work closely follows the approach of Abarca (2013), yielding results that are presented in a similar way to the previous results to allow comparison.

One difference is that two new shoreline positions are considered, representing the situation at 2500 AD and 3500 AD in the "global warming" and "early periglacial" climate scenarios, in place of a case at 3000 AD in the previous work. The correspondence between shoreline positions considered in the two versions of the model is summarized in Table 4.1. The positions considered in the updated model are shown in Figure 4.2.

Table 4.1: Comparison of shoreline positions previously modelled by Abarca et al. (2013) versus. positions treated in the updated model of Abarca et al. (2019).

Time	Shoreline positions previously modelled*	Shoreline positions in updated model	Description of situation
2000 AD	Position 1 _o	Position 1	Repository submerged
2500 AD	--	Position 2	Shoreline right over SFR 1 and SFR 3
3000 AD	Position 2 _o	--	Shoreline slightly north of the repository
3500 AD	--	Position 3	Shoreline has moved north away from the repository.
5000 AD	Position 3 _o	Position 4	Shoreline still retreating and well removed from the repository.

* To reduce potential for confusion, in this review a subscripted letter o will be used to distinguish positions evaluated with the older model.

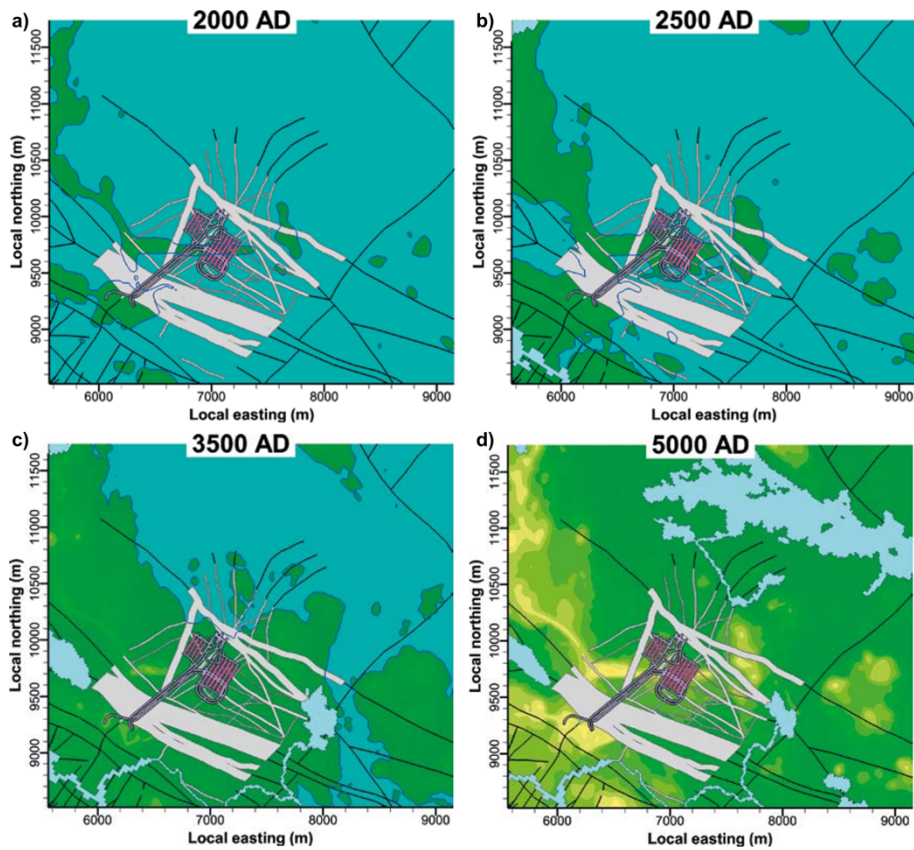


Figure 4.2: Shoreline positions with respect to the SFR repository. From Figure 3-10 of Abarca et al. (2019).

4.2. Results from updated model for SFR 1

For SFR 1, the calculated flows from the updated model, both through the vaults as a whole, and through waste compartments within the vaults, are generally very close to the values from the previous model of Abarca et al. (2013). The ratios of flows for the updated model relative to the previous model are given in Table 4.2. Except for 1BTF where the flow is increased by 37%, the values are within 15% of the previous results.

Table 4.2: Ratios of the total flow through the SFR 1 vaults with respect to the Base case in Abarca et al. (2013). Ratios lower than one indicate a reduction in the total flow with respect to the flows reported in Abarca et al. (2013). From Table 4-2 of Abarca et al. (2020).

Ratio		2000 AD	5000 AD
Vaults	1BMA	0.95	0.88
	1BLA	0.92	0.91
	1BTF	1.03	1.37
	2BTF	0.91	1.03
	Silo*	0.92	0.88
Waste	1BMA	0.86	1.04
	1BLA	0.96	0.94
	1BTF	1.05	1.14
	2BTF	1.02	1.12
	Silo*	0.89	0.95

*The Silo vault does not include the gravel dome.

As in Abarca et al. (2013), the effects of concrete degradation have been studied with a set of three simulations referred to as moderate, severe, and complete concrete degradation. Results given graphically and numerically in Figures 4-5 and Figures 4-8 of Abarca et al. (2019), for the shoreline positions at 2000 AD and 5000 AD are very similar to the corresponding results from the previous model.

Likewise, previous calculations for three plug degradation cases (moderate, severe, and complete plug degradation) were repeated with the updated model and gave very similar results. In the most extreme case of complete plug degradation, the change in flow through most of the SFR 1 vaults is less than 10% except for 1BTF and 2BTF. Flows through the waste are much less strongly affected, with a 4% increase in 1BLA and lesser effects in the others.

The case of "no barriers" (meaning simultaneous complete degradation of the concrete barriers and bentonite barriers) from the previous model is also repeated with the updated model. The effects seen in the updated model are similar to those for the previous model, with flows through the Silo increasing by three orders of magnitude but lesser effects in the other vaults of SFR 1.

Likewise similar results to the previous model are obtained for a scenario in which an ice lens is assumed to develop in the Silo and produce a degradation of the bentonite.

Uncertainty in the geosphere has been addressed only with the same two realizations of Odén et al. (2013) as used previously, so there is no extension of the work on this issue.

An alternative initial state not considered by Abarca et al. (2013) was evaluated as a new calculation case with the updated model. This considers the potential reduction of flow in the 1BMA and 2BMA vaults by using a high-performance construction

concrete. This has only a minor effect on flow through the 1BMA and 2BMA vaults in SFR 1, relative to the Base case. However flow through the waste in 1BMA is reduced by up to 88% in the initial period, with a sustained reduction of 38% through 5000 AD. The effect of high-performance concrete on flow through the waste in 2BMA is even more pronounced, with a reduction of nearly two orders of magnitude throughout the analysed period.

4.3. Results from updated model for SFR 3

Results for the updated model of SFR 3 generally follow along the same lines as discussed for SFR 1, in the previous section. The largest difference is that the significantly increased dimensions of BRT result in a 67% increase in flow relative to the previous model, for the Base case at 2000 AD. This result is reasonable as it is roughly in proportion to the increase in the cross-sectional area of the BRT vault. The prediction of generally smaller impacts for the other waste vaults is also reasonable, considering that the changes in geometry are comparatively small.

For both SFR 1 and SFR 3, the predictions of Abarca et al. (2019) regarding impacts of the changes in vault dimensions and engineered barriers are well explained and generally concordant with what should be expected. A further check on the reasonableness of these results is recommended to confirm this qualitative assessment. This can be done by updating previous calculations based on a simplified representative model (Geier et al., 2019), taking into account the changes in vault dimensions and properties.

5. Summary of main findings

The main findings from this review are summarized below in terms of the main categories of reports that have been considered.

5.1. Modelling of glacial and periglacial conditions

Recent modelling of glacial and periglacial situations based on the Greenland Analogue Project (GAP) demonstrates the possibility to treat multiple coupled processes including density-dependent groundwater flow, heat flow, formation and melting of permafrost, and advective-dispersive transport of salinity. These developments represent advances in SKB's capability to treat most of the major physical processes that are expected to be relevant for groundwater flow in glacial and periglacial situations, although at this point there are still difficulties in representing matrix diffusion.

Concepts and methods for representing flow of glacial meltwater at the ice/bedrock interface have also been developed and applied within these exercises. Thus far these representations are speculative and have not yet been demonstrated to reproduce the types of flow behaviour documented by the Greenland ICE project subsequent to GAP (Harper et al., 2021).

The significance of glacial and periglacial situations for repository safety assessment may be diminished in view of the continuing lack of success to rein in global anthropogenic carbon emissions. For a relatively high-emissions scenario that increasingly appear more likely, climate evolution modelling by Lord et al. (2019) and Williams et al. (2022) predicts that the next glacial inception could be delayed until about 170,000 years from present, and the first ice sheet coverage at Forsmark would not occur until around 410,000 years from present.

The model of Jaquet et al. (2019) predicts very deep penetration of dilute meltwaters during glacial retreat. However, the model as applied does not include the effects of matrix diffusion (due to numerical difficulties), and includes rather unrealistically high values of hydraulic conductivity, which may lead to exaggeration of groundwater circulation to depth. Scoping calculations based on analytical approaches are recommended to investigate the potential impacts of these effects.

The models give some insight into the potential role of taliks (areas of unfrozen ground in permafrost) as potential sites for focused discharge and possibly also recharge. The representation of taliks is artificial, by imposing a fixed temperature on locations of known taliks. However based on limited results of Cohen-Corticchiato and Zwinger (2021) for the Finnish repository programme, using a model that includes a mechanism for taliks to form dynamically, the assumption that talik locations are stable appears to be a reasonable simplification.

5.2. Developments in DFN methods

In addition to a report summarizing SKB's overall DFN methodology (in two volumes, of which only the first volume has been published to date), specific

developments in the methodology include (1) demonstration of DFN conditioning methods, (2) incorporation of rock stress effects on hydraulic properties of fractures, and (3) influence of fracture heterogeneity on network-scale transport. The main findings on these topics are summarized in sequence below.

5.2.1. Demonstration of DFN conditioning methods

Two separate modelling groups using different proprietary software (ConnectFlow and FracMan) participated in a joint project called DFN-R, to demonstrate methods for conditional simulation of DFN statistical models for the types of situations that are expected to arise during repository construction.

A "synthetic reality" is constructed as a simulation of a DFN statistical model, then used to simulate the types of data that will be available during successive stages of repository construction, including (1) excavation of a main transport tunnel, (2) drilling of horizontal pilot holes for deposition tunnels, (3) excavation of the deposition tunnels, (4) drilling of vertical pilot holes for the deposition holes, and finally (5) boring of the deposition holes.

The two modelling groups used substantially different algorithms and based their conditional simulations on different subsets of the synthetic data. Both demonstrated the capacity to integrate the main types of anticipated data into their models in a way that honours the geometry of intersections between fractures and underground openings, and flow measurements in pilot holes.

The FracMan group (Bym and Hermanson, 2017) used only the subset of the data that would be available prior to drilling pilot holes for the deposition holes. This gave only limited improvement in predicting flows to deposition holes, relative to an unconditioned DFN model.

The ConnectFlow group (Appleyard et al., 2017) used all data up through drilling of pilot holes for deposition holes, and not surprisingly had better success in terms of predicting flows to the actual deposition holes during the construction period. Further conditioning based on observed flows to deposition holes during construction gave improved predictions of post-closure flows U and transport resistance F relative to models with lesser degrees of conditioning, but uncertainty remains high (though generally on the conservative side) both for U and F .

It should be noted that all of these results are based on a situation where the DFN statistical model is known perfectly *a priori*, and reality conforms to the idealized assumptions of the statistical model (including homogeneous hydraulic properties within each fracture). Hence, errors resulting from the process of statistical inference and/or from channelling effects within heterogeneous fractures, which might add significantly to the prediction error for these post-closure flow-related performance measures, are not accounted for in this exercise.

5.2.2. Coupling of DFN models to hydraulic stresses

Another DFN study by Hartley, et al. (2021) is a comprehensive re-interpretation of fracture data from Forsmark, including new data from the shallow bedrock as well

as older data on sheet joints that are thought to be related to the strongly anisotropic, highly conductive "shallow bedrock aquifer."

This is a significant update of the Forsmark bedrock hydrogeological model compared with the model for SR-Site. A key feature is that, by incorporating the effects of rock stresses on fracture aperture, it points toward an integrated DFN description of shallow and deep bedrock at Forsmark, including sheet joints created and/or dilated by vertical stress relief in the shallow bedrock.

One feature still lacking from this model is the geological observation of "sand dikes" as noted during mapping by Carlsson (1979), presumably injected under very high hydraulic gradients during past glaciations. Glaciofluvial sediments have been found in sheet joints at Forsmark down to about 50 m depth (Follin et al., 2007). Such sediments may keep some of these near-surface sheet joints propped open and able to sustain very high flows, independent of stress. The recent ICE project (Harper et al., 2021) investigated dynamic flow processes at the base a receding glacier and may provide further insights into conditions that could give rise to this phenomenon.

5.2.3. Effects of fracture heterogeneity on transport

The numerical study of Bym and Follin (2019), also based on synthetic data, tested whether a flow-calibrated DFN model with homogeneous fractures can reproduce the particle tracking (transport) behaviour of a DFN model with channelling due to heterogeneous fractures. The results indicate that the homogeneous DFN model is generally non-conservative for predicting transport, even after calibration to PFL measurements.

This seemingly contradicts earlier work by Painter and Cvetkovic (2001) and Painter (2006), who concluded that within-fracture aperture variability contributes little to field-scale transport because it is overwhelmed by the much larger fracture-to-fracture variability. However there are key differences between the models, in terms of the representation of intrafracture heterogeneity.

The model of Bym and Follin (2019) is more strongly channelized within fractures than the earlier models. Their model also accounts for the possibility of errors that might occur in calibrating a homogeneous-fracture model to PFL measurements in a system of heterogeneous fractures, which is a problem that exists in reality. The finding that calibration of a homogeneous-fracture model to flow data from a channelized fracture system could lead to non-conservatism suggests that this issue needs further consideration.

5.3. Near-field modelling for SR-PSU

The last major topic considered in this review was an updated model of the SFR by Abarca et al. (2019). This is a rather minor update of previous calculations, taking into account potential modifications mainly in the properties of concrete structures in the existing SFR 1 waste vaults, and changes in the dimensions and properties of

the proposed SFR 3 expansion. The results are well presented, in a way that generally allows for direct comparison with the results of the previous model.

The predicted impacts of the changes in vault dimensions and engineered barriers are well explained and generally concordant with what should be expected. An update of simple representative model calculations (Geier et al., 2019) is suggested to check the sensitivity of predictions to these changes, although it is expected that the impacts of changes will be minor.

6. References

(*) indicates reports reviewed here.

Abarca, E., A. Idiart, L.M. de Vries, O. Silva, J. Molinero J, and H. von Schenck, 2013. Flow modelling on the repository scale for the safety assessment SR-PSU. SKB TR-13-08, Swedish Nuclear Fuel and Waste Management Co.

Abarca, E., O. Silva, a. Idiart, A. Nardi, J. Font, and J. Molinero, 2014. Flow and transport modelling on the vault scale for the safety assessment SR-PSU. SKB R-14-14, Swedish Nuclear Fuel and Waste Management Co.

* Abarca, E., D. Sampietro, J. Sanglas, and J. Molinero, 2019. Modelling of the near-field hydrogeology – Report for the safety assessment SR-PSU (PSAR). SKB R-19-20, Swedish Nuclear Fuel and Waste Management Co.

Applegate, D., P. Appleyard, and S. Joyce, 2020. Modelling solute transport and water-rock interactions in discrete fracture networks. Posiva Working Report 2020-01, Posiva Oy.

* Appleyard, P., P. Jackson, S. Joyce, and L. Hartley, 2017. Conditioning DFN models on intersection, connectivity and flow data. SKB-R-17-11, Swedish Nuclear Fuel and Waste Management Co.

Black, J.H., N.D. Woodman, , and J.A. Barker, 2017. Groundwater flow into underground openings in fractured crystalline rocks: an interpretation based on long channels. *Hydrogeology Journal*, v. 25, p. 445-463. <https://doi.org/10.1007/s10040-016-1511-y>

Black, J.H. and J.A. Barker, 2018. An alternative approach to understanding groundwater flow in sparse channel networks supported by evidence from 'background' fractured crystalline rocks. *Hydrogeology Journal* v. 26, p. 2707–2723. <https://doi.org/10.1007/s10040-018-1823-1>.

* Bym, T. and S. Follin, 2019 A numerical study of channelling in heterogeneous versus calibrated homogeneous DFN realisations. SKB-R-19-24, Swedish Nuclear Fuel and Waste Management Co.

* Bym, T., and J. Hermanson. Methods and workflow for geometric and hydraulic conditioning. DFN-R – status report 2013–2015. SKB-R-17-12, Swedish Nuclear Fuel and Waste Management Co.

Caine, J. S., J. P. Evans and C. B. Forster, 1996. Fault zone architecture and permeability structure. *Geology* v. 24, p. 1025-1028.

Carlsson A, 1979. Characteristic features of a superficial rock mass in southern central Sweden: horizontal and subhorizontal fractures and filling material. PhD thesis. Uppsala University, Sweden.

* Cohen-Corticchiato, D. and T. Zwinger, June 2021 . Modelling permafrost evolution at Olkiluoto for the next 120,000 years. Posiva Working Report 2021-14, Posiva Oy.

Claesson Liljedahl, L., A., Kontula, J. Harper, J-O. Näslund, J-O Selroos, P. Pitkänen, I. Puigdomenech, M. Hobbs, S. Follin, S. Hirschorn, L., Kennel, N.

- Marcos, T. Ruskeeniemi, E-L. Tullborg, and P. Vidstrand, 2016. The Greenland Analogue Project: Final report. SKB TR-14-13, Swedish Nuclear Fuel and Waste Management Co.
- Dessirier, B., C-F. Tsang, and A. Niemi, 2018. A new scripting library for modeling flow and transport in fractured rock with channel networks. *Computers & Geosciences* 111, 181–189.
- Doherty, J., 2015. *Calibration and Uncertainty Analysis for Complex Environmental Models*. Watermark Numerical Computing, Brisbane, Australia. ISBN: 978-0-9943786-0-6.
- Geier, J., 2017. Review of hydrogeological aspects of SR-PSU – main review phase. In SSM Report 2017:28, Swedish Radiation Safety Authority, Stockholm.
- Geier, J.E., Lindgren, G.A., and Tsang, C-F., 2019. Simplified representative models for long-term flow and advective transport in fractured crystalline bedrock. *Hydrogeology Journal*, v. 27, n. 2, p. 595-614. <https://doi.org/10.1007/s10040-018-1875-2>.
- Harper, J., A. Hubbard, T. Ruskeeniemi, L. Claesson Liljedahl, A. Kontula, M. Hobbs, J. Brown, A. Dirkson, C. Dow, S. Doyle, H. Drake, J., Engström, A. Fitzpatrick, S. Follin, S. Frape, J. Graly, K. Hansson, J., Harrington, E. Henkemans, S. Hirschorn, N. Humphrey, P. Jansson, J. Johnson, G. Jones, P. Kinnbom, L. Kennell, K.E. Klint, J. Liimatainen, K., Lindbäck, T. Meierbachtol, T. Pere, R. Pettersson, E-L. Tullborg, and D. van As, 2016. The Greenland Analogue Project: Data and processes. SKB R-14-13, Swedish Nuclear Fuel and Waste Management Co.
- Dansgaard, W., S.J. Johnsen, H.B. Clausen, D. Dahl-Jensen, N.S. Gundestrup, C.U., Hammer, C.S. Hvidberg, J.P. Steffensen, A.E. Sveinbjörnsdóttir, J. Jouzel, and G. Bond, 1993. Evidence for general instability of past climate from a 250-kyr ice-core record. *Nature* 364, 218–220.
- Follin, S., J., Levén, L Hartley, P. Jackson, S. Joyce, D. Roberts, and B. Swift, 2007. Hydrogeological characterisation and modelling of deformation zones and fracture domains, Forsmark modelling stage 2.2. SKB R-07-48, Swedish Nuclear Fuel and Waste Management Co.
- Fox, A., P. La Pointe, J., Hermanson, J., and Öhman, 2007. Statistical geological discrete fracture network model. Forsmark modelling stage 2.2. SKB R-07-46, Swedish Nuclear Fuel and Waste Management Co.
- Harper, J., T. Meierbachtol, and N. Humphrey, 2021. Posiva Working Report 2019-17: Greenland ICE Project -- Final Report. Posiva Oy.
- Hartley, L., S. Baxter, and T. Williams, 2016. Geomechanical Coupled Flow in Fractures during Temperate and Glacial Conditions. Posiva Working Report 2016-08. Posiva Oy.
- * Hartley, L., S. Baxter, J. Carty, and S. Libby, 2021. Exploratory integration of DFN models and 1D stress models with data from hydraulic tests for the shallow bedrock at the Forsmark site. SKB-R-21-13, Swedish Nuclear Fuel and Waste Management Co.

- Jaquet, O., R. Namar, and P. Jansson, 2010. Groundwater flow modelling under ice sheet conditions. Scoping calculations. SKB R-10-46, Swedish Nuclear Fuel and Waste Management Co.
- Jaquet, O., R. Namar, P. Siegel, and P. Jansson, 2012. Groundwater flow modelling under ice sheet conditions in Greenland (phase II). SKB R-12-14, Swedish Nuclear Fuel and Waste Management Co.
- * Jaquet, O., R. Namar, P.l Siegel, J. Harper, and P. Jansson 2019. Groundwater flow modelling under transient ice sheet conditions in Greenland. SKB-R-19-17, Swedish Nuclear Fuel and Waste Management Co.
- Johnsen, S.J., H.B. Clausen, W. Dansgaard, N.S. Gundestrup, C.U. Hammer, U. Andersen, K.K. Andersen, C.S. Hvidberg, D. Dahl-Jensen, J.P. Steffensen, H. Shoji, E. Sveinbjörnsdóttir, J.W. White, J. Jouzel, and D. Fisher, 1997. The $\delta^{18}O$ record along the Greenland Ice Core project deep ice core and the problem of possible Eemian climatic instability. *Journal of Geophysical Research* 102, 26397–26410.
- Lord, N.S., D. Lunt, and M. Thorne, 2019. Modelling changes in climate over the next 1 million years. SKB Technical Report TR-19-09, Swedish Nuclear Fuel and Waste Management Co.
- Painter, S., and V. Cvetkovic, 2001. Stochastic analysis of early tracer arrival in a segmented fracture pathway, *Water Resources Research*, 37(6), 1,669–1,680.
- Painter, S., 2006. Effect of single-fracture aperture variability on field-scale transport. SKB Report R-06-25, Swedish Nuclear Fuel and Waste Management Co.
- Selroos, J-O., Mas Ivars, D., Munier, R., Hartley, L., Libby, S., Davy, P., Darcel, C., and Trincherro, P., 2022. Methodology for discrete fracture network modelling of the Forsmark site. Part 1 – concepts, data and interpretation methods. SKB-R-20-11, Swedish Nuclear Fuel and Waste Management Co.
- Shahkarami, P. and Sidborn, M., 2023. Simulation of Helium transport in fractured rocks: Implementation of a dual continuum model in DarcyTools. *Journal of Contaminant Hydrology* v. 253 (104123), <https://doi.org/10.1016/j.jconhyd.2022.104123>
- Williams, C.J.R , D.J. Lunt, A.T. Kennedy-Asser, and N.S. Lord, 2022. Uncertainties in modelled climate changes at Forsmark over the next 1 million years. SKB Technical Report TR-22-02, Swedish Nuclear Fuel and Waste Management Co.
- * Vidstrand, P., 2017. Concept testing and site-scale groundwater flow modelling of the ice sheet marginal-area of the Kangerlussuaq region, Western Greenland. SKB-R-15-01, Swedish Nuclear Fuel and Waste Management Co.
- Zinn, B., and C.F. Harvey, 2003. When good statistical models of aquifer heterogeneity go bad: A comparison of flow, dispersion, and mass transfer in connected and multivariate Gaussian hydraulic conductivity fields. *Water Resources Research* 39(3), 1051, doi:10.1029/2001WR001146.

The Swedish Radiation Safety Authority (SSM) works proactively and preventively with nuclear safety, radiation protection, nuclear security, and nuclear non-proliferation to protect people and the environment from the harmful effects of radiation, now and in the future.

You can download our publications from www.stralsakerhetsmyndigheten.se/en/publications. If you need alternative formats such as easy-to-read, Braille or Daisy, contact us by email at registrator@ssm.se.

Strålsäkerhetsmyndigheten

SE-171 16 Stockholm
+46 (0) 8-799 40 00
www.stralsakerhetsmyndigheten.se
registrator@ssm.se

©Strålsäkerhetsmyndigheten
Rapportnummer: 2024:13
ISSN: 2000-0456